Journal of
Materials Chemistry B

Materials for biology and medicine
www.rsc.org/MaterialsB

ISSN 2050-750X

PAPER
Mariana Pinteala et al.
Flexible cyclic siloxane core enhances the transfection e ciency of polyethylenimine-based non-viral gene vectors

This manuscript was published as formal in:
J Mater Chem B, 2015, 3, 8250-8267
https://doi.org/10.1039/c5tb01342a

Journal of
Materials Chemistry B

PAPER

Flexible cyclic siloxane core enhances the transfection efficiency of polyethylenimine-based non-viral gene vectors†

Cite this: DOI: 10.1039/c5tb01342a

Cristina M. Uritu,[a] Manuela Calin,[b] Stelian S. Maier,[ac] Corneliu Cojocaru,[a] Alina Nicolescu,[a] Dragos Peptanariu,[a] Cristina Ana Constantinescu,[b] Daniela Stan,[b] Mihail Barboiu[d] and Mariana Pinteala*[a]

Received 6th July 2015,
Accepted 17th August 2015

DOI: 10.1039/c5tb01342a

www.rsc.org/MaterialsB

Transfection of nucleic acid molecules, large enough to interfere with the genetic mechanisms of active cells, can be performed by means of small carriers, able to collectively collaborate in generating cargocomplexes that could be involved in passive mechanisms of cellular uptake. The present work describes the synthesis, characterization, and evaluation of transfection efficacy of a conjugate molecule, which comprises a cyclic siloxane ring (2,4,6,8-tetramethylcyclotetrasiloxane, cD_4^H) as the core, and, on average, 3.76 molecules of 2 kDa polyethyleneimine (PEI) as cationic branches, with an average molecular mass of 7.3 kDa. As demonstrated by *in silico* molecular modeling and dynamic simulation, the conjugate molecule (cD_4^H–AGE–PEI) tends to adopt an asymmetric structure, specific for amphipathic molecules (confirmed by a log *P* value of −1.902 ± 0.06), that favors a rapid interaction with nucleic acids. The conjugate and the polyplexes with the pEYFP plasmid were proved to be non-cytotoxic, and capable of ensuring transfection yields better than 30%, on HEK 293T cell culture, superior to the value obtained using the SuperFect® reagent. We presume that the increased transfection efficacy originates in the ability of the conjugate to locally tightly encompass pDNA molecules by electrostatic interaction mediated by the short PEI branches, and consequently to expose the siloxane hydrophobic moiety, which decreases the interaction energy with the lipid layers.

Introduction

Regardless of their nature and type, gene vectors must be able to pass through physiological barriers, and need to fight against the cells' defensive systems, which are able to detect and silence the "intruder" DNA.[1] In addition, synthetic DNA carriers must be able to pack or wrap genetically significant segments of DNA, of more than 27 kilobases, which is the average dimension of a human active gene that contains introns too.[2]

Carrying and targeted delivery of large segments of nucleic acids is proved to be efficient when viral vectors are used,[3] but still represents a challenge in producing and using non-viral gene vectors. In principle, there are no size limitations in the case of cationic lipid-based vectors,[4] but evident drawbacks have been revealed when liposomes were applied to deliver DNA into cells (poor transfection efficiency, poor entrapment stability in *in vivo* conditions,[5] short lifetime, inactivation by serum proteins, cytotoxicity of cationic lipids in large amounts, especially on phagocytes[6]). If they are non-cytotoxic, nanometric sized particulate polycationic entities,[7,8] possibly endowed with cell penetrating[9,10] and active targeting[11] components, decorated with protectant molecules,[12] and featured with stimuli responsiveness,[13,14] are feasible DNA carriers, both as individual particles, and as collectively encapsulated ones.[15,16]

Spatially extended cargocomplexes generated by the electrostatic self-assembly between numerous individual carrier entities and the DNA segments might represent a practical solution to deliver genes and plasmids of large size. In this respect, different chemical architectures of the individual polymeric cationic carriers were tested, in the pursuit of smaller

[a] *Centre of Advanced Research in Bionanoconjugates and Biopolymers, "Petru Poni" Institute of Macromolecular Chemistry, Iasi, 700487, Romania*
[b] *"Nicolae Simionescu" Institute of Cellular Biology and Pathology of the Romanian Academy, Bucharest, 050568, Romania*
[c] *"Gheorghe Asachi" Technical University of Iasi, Iasi, 700050, Romania*
[d] *Adaptative Supramolecular Nanosystems Group, Institut Européen des Membranes, ENSCM/UMII/UMR-CNRS 5635, 34095 Montpellier, Cedex 5, France*

† Electronic supplementary information (ESI) available: Additional experimental data of cD_4^H–AGE–PEI conjugate and its precursors including FTIR spectra, XPS wide scan spectra, a table resuming high resolution spectra C 1s and N 1s assignments, TGA/DTG and DSC curves, a table comprising summary results of molecular dynamics simulation regarding DNA/cD_4^H–AGE–PEI. See DOI: 10.1039/c5tb01342a

dimensions accompanied by stable unfolded states of the macromolecular chains. These architectures mainly differ in terms of structural ordering (the "rigidity" of their edifice), and of the presence of local cores ("articulating points") consisting of small functional chains or freestanding molecules. The first category comprises dendrimers[17,18] and dendrimeric-type branched macromolecules.[19] The second one is far more diversified, comprising less- or no-ordered structures, and includes independent linear or branched cationic macromolecules,[20] and polycations "articulated" on (low-)molecular local cores, such as fullerenes[21,22] and cyclodextrin,[23–25] or on relatively complex molecules, like the hyperbranched poly(arylene oxindole).[26]

The present work proposes the use of a cyclic siloxane as the local core of a new DNA carrier of nanometric dimensions that is able to collectively participate in the electrostatic complexation of DNA to form extended cargocomplexes. Tetramethylcyclotetrasiloxane, a four unit siloxane ring of general formula $(CH_3)_nO_nH_nSi_n$ (where $n = 4$), further named cD_4^H, was chosen due to its lack of cytotoxicity when used in trace amounts,[27] low (bio)chemical reactivity, high hydrophobicity, and low surface tension.[28]

Siloxane containing gene vectors, prepared according to the principles described in ref. 29, proved to be able to penetrate the blood–brain barrier,[30] and to deliver calcitonin gene-related peptide (CGRP) gene,[31] which is active in attenuating cerebral vasospasm in rats affected by subarachnoid hemorrhage. However, to the best of our knowledge, the literature does not report the use of cyclic siloxane as a core of nucleic acid carriers. The new non-viral gene vector architecture that we designed

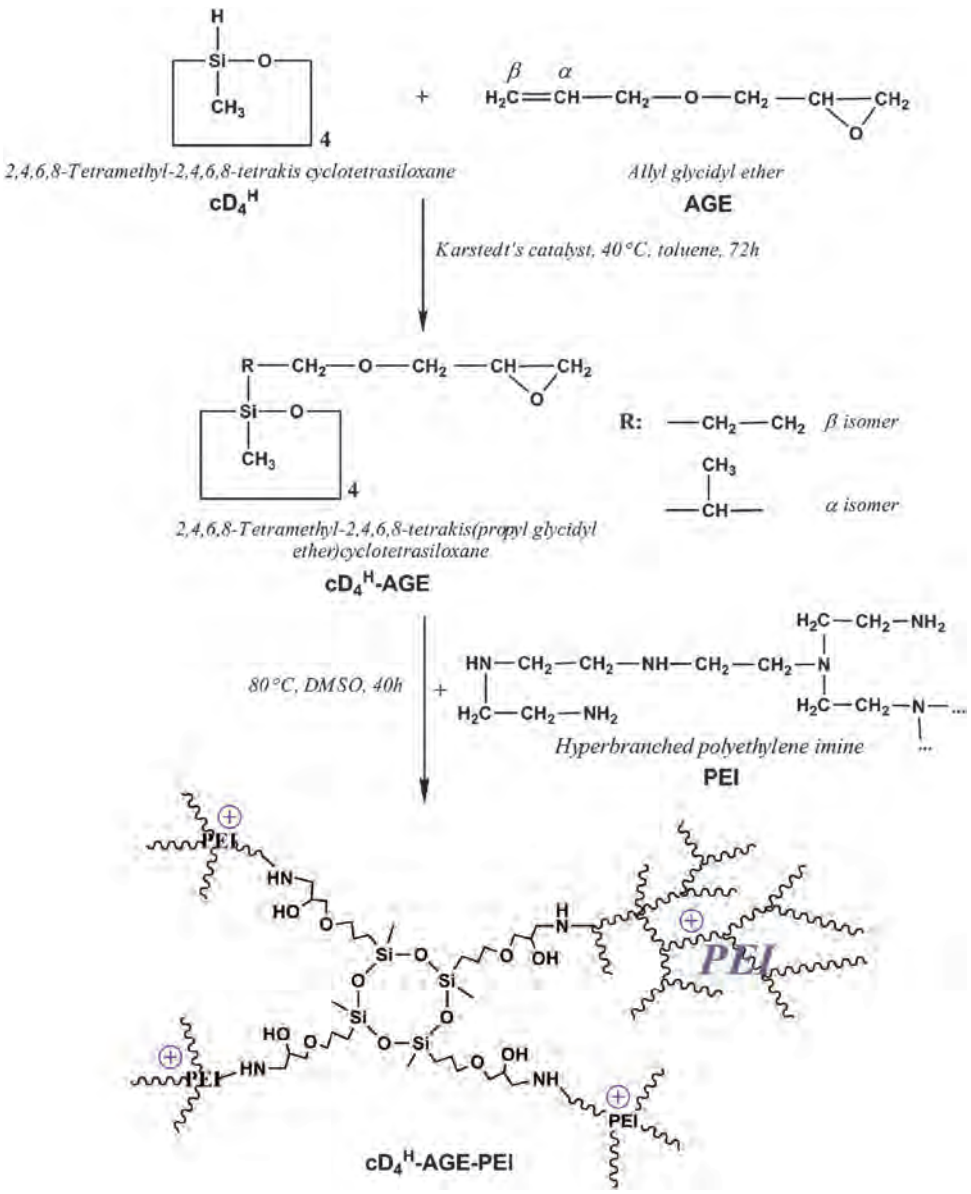

Scheme 1 The two-step synthesis of the silicone-core based carriers.

benefits from the hydrophobicity of the siloxane core, a peculiar property that has been recently related to the increase of transfection efficacy.[32]

The use of cD_4^H as the core of the DNA carriers exploits its high ring flexibility[33] (which is due to the low barrier energy of the Si–O–Si bond deformation, and of Si–O bond rotation, concluded by a high conformational interconversion ability and rate), that enhances the propensity of the carrier edifice to adopt the most favorable conformation during the electrostatic complexation with nucleic acids, thus maximizing the compactness and minimizing the dimension of the resulted polyplexes. In addition to this, based on the similar reported results,[34] it is presumable that, as cores of the carriers, cD_4^H will contribute by its hydrophobicity to the enhancement of the transfection efficiency of the cargocomplexes.

The involvement of silicon compounds in organic synthesis allows us to benefit from three of its reactivity peculiarities: (i) its lower electronegativity as compared to carbon,[35] (ii) its ability to temporarily increase its covalency during the reaction pathway, up to penta- or even hexa-valency,[36] and (iii) the opposite polarisation of $Si^{\delta+}$–$H^{\delta-}$ bonds in comparison to $C^{\delta-}$–$H^{\delta+}$ ones.[37] As a consequence, nucleophilic attack will always occur at silicon atoms inside an organic molecule, and vinyl systems preferentially add to tetra-valent enchained silicon atoms. Based on these reactivity aspects, cD_4^H can be precisely and reproducibly derivatized, which allows us to synthesize tailored reaction product molecules.

Results

The carrier synthesis and characterization

The cD_4^H–AGE precursor was obtained by hydrosilation of allyl glycidyl ether with cD_4^H, in the presence of Karstedt's catalyst, at 40 °C, in toluene (Scheme 1). After removing the solvent, the AGE excess and the catalyst, the resulting reaction product was a mixture of α- and β-isomers in a 1 : 29 molar ratio (3.4% α-isomer), as calculated from the ^{1}H-NMR spectrum (Fig. 1a). To quantitate the isomers, the values of the integrated characteristic peaks (δ around 1.00 ppm, specific to CH_3–CH–Si protons of α-isomer, and δ around 0.61 and 1.66 ppm, specific to –CH_2–CH_2–Si and –CH_2–CH_2–Si protons, respectively, of β-isomer), were taken into consideration. Being a derivative of chloroplatinic acid, Karstedt's catalyst is able to promote hydrosilation at temperatures below 50 °C, with no byproduct formation, and at a molar ratio favorable to the β-isomer, as compared with the H_2PtCl_6 catalyst operating at 100 °C, when a molar ratio of 1 : 9 between α- and β-isomers results.[38] The carbon chemical shift values also sustain the formation of the desired reaction product (see Fig. 1a′). The progress of the hydrosilation reaction was monitored in FTIR spectroscopy, by observing the disappearance of the strong silicone hydride stretching band (Si–H) at around 2170 cm^{-1}, showing the total consumption of the Si–H groups. Completion of the reaction after about 72 h was confirmed by ^{1}H NMR spectrum (not shown), when the disappearance of the Si–H bond at a chemical shift of 4.86 ppm becomes evident, and is accompanied by the modifying of other specific peaks.

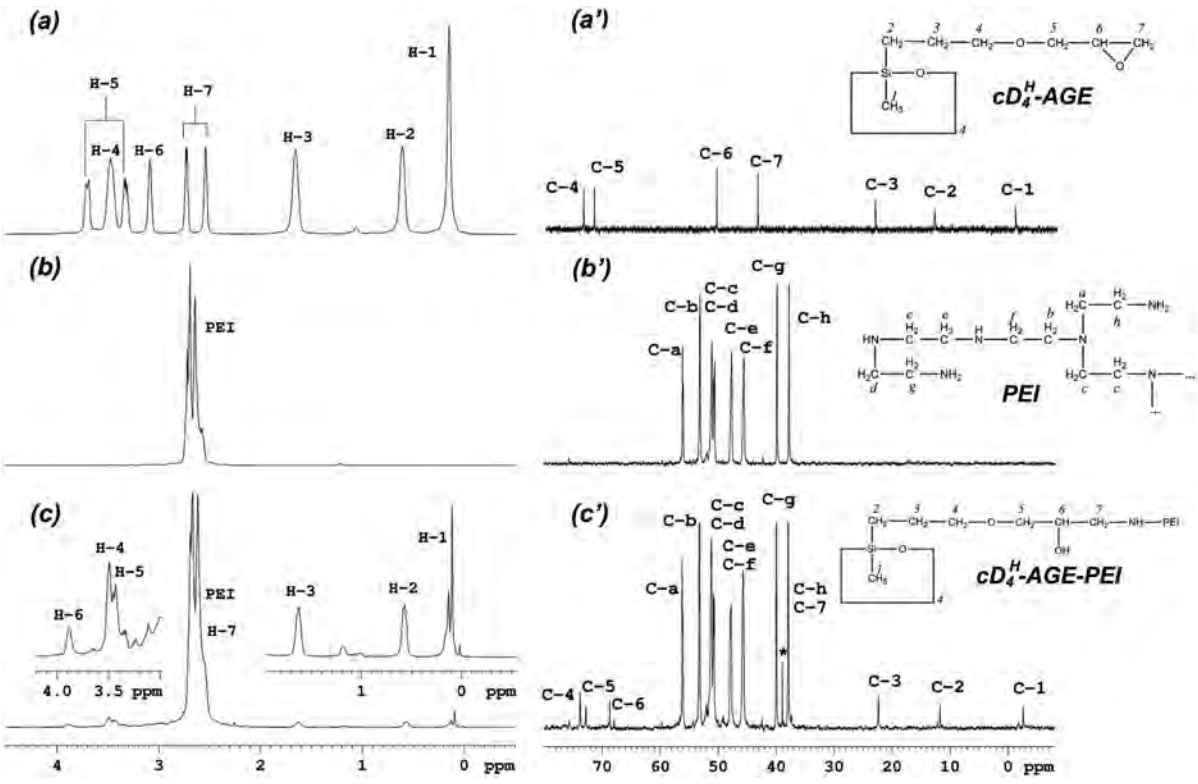

Fig. 1 The ^{1}H and ^{13}C NMR spectra of the cD_4^H–AGE and PEI precursors, and of the cD_4^H–AGE–PEI conjugate.

The cD_4^H–AGE–PEI carrier molecule was further synthesized by the conjugation of the cD_4^H–AGE precursor with branched PEI oligomer molecules, by the ring-opening reaction of the AGE oxirane terminal group.[38] Stoichiometrically, a dendrimer like molecule results, which has a cyclotetrasiloxane core, grafted with four PEI molecules. The reaction occurred in DMSO, at 80 °C, for 40 hours, in the presence of isopropanol, which acts as an activating agent for the ring-opening reaction, and as a blocker of the potential reaction between the emerging OH groups and the AGE oxirane ring. The ^{1}H-NMR spectrum provides evidence for the structure of the cD_4^H–AGE–PEI conjugate (Fig. 1c), and provides its approximate molecular weight through the integrated values of the characteristics peaks. The reaction between the cD_4^H–AGE precursor and PEI at a molar ratio of 1 : 4 induces the formation of (typically four) N–C bonds. Conjugation progress is demonstrated by the fading (and disappearance) of the characteristic peaks of the oxirane cycle (at 2.58, 2.78, and 3.08 ppm), concomitantly with the appearance of and increase in the C*H*–OH and CH_2–NH–PEI specific peaks, at 3.88 ppm, and in the range of 3.33 to 3.49 ppm, respectively (Fig. 1a and c), but the CH_2–NH–PEI peak overlaps with CH_2–O protons from the ether bond of AGE. ^{13}C NMR spectroscopy (Fig. 1a′) also reveals the consumption of oxirane groups, expressed by the shifts of peaks at 43.46 (C7) and 50.56 (C8) ppm in the cD_4^H–AGE precursor. The formation of the cD_4^H–AGE–PEI conjugate is clearly evidenced by the ^{13}C NMR spectrum, where the new signals at 67.94 and 68.70 ppm are attributed to –*C*H$_2$–CH(OH) –*C*H$_2$–, and –*C*H–OH atoms, respectively, and the peak at 38.93 ppm belongs to the carbon atom from the new –*C*H$_2$–N– bond (Fig. 1c′). The corresponding signals of PEI exhibit obvious changes in morphology and intensity in the range of 30–60 ppm after conjugation with the cD_4^H–AGE precursor (see Fig. 1b′ and c′).

Based on ^{1}H NMR data processing performed by calculating the ratios of peaks integrals corresponding to the newly formed –C*H*(OH)– groups and to the CH_3–Si moiety (see Scheme 1 and the spectrum description at the end of the synthesis protocols), the cD_4^H–AGE–PEI conjugate contains, on average, 3.76 molecules of PEI per siloxane core cycle. This value results as follows. The experimentally determined integrals of the protons of the –C*H*(OH)– and CH_3–Si groups were 0.6 and 1.91, respectively. Considering that the unit absorption of methyl protons is 0.637 (=1.91/3), the abundance ratio of the –C*H*(OH)– and CH_3–Si groups is 0.94 (=0.6/0.637). Therefore, because the cD_4^H cycle contains four Si atoms, the number of newly generated –C*H*(OH)– groups corresponding to each cycle is 3.76 (=0.94 × 4).

FTIR spectra of the cD_4^H–AGE–PEI conjugate, the cD_4^H–AGE precursor and their originating reagents are presented in Fig. S1, in the ESI.† It is obvious that the hydrosilation step concludes with the total depletion of the Si–H peak at 2175 cm^{-1}, confirming the stoichiometric grafting of cD_4^H with AGE molecules. The presence of the oxirane group is revealed in the cD_4^H–AGE spectrum by the strong symmetric stretching vibration at 910 cm^{-1}, and an asymmetric stretching vibration at 1259 cm^{-1}.[39] The Si–CH$_3$ specific band at 804 cm^{-1} is also present, alongside the peaks of siloxanic bonds at 1000–1100 cm^{-1}, and of ether groups at 2933 cm^{-1} and 1479 cm^{-1}. The weak peaks at 2758 cm^{-1} and 3053 cm^{-1} could be explained by the presence of residual traces of AGE in the investigated precursor sample. The peak at 2997 cm^{-1} could have its origin in –CH$_3$ groups of cD_4^H.

The FTIR spectrum of PEI displays the characteristic bands for primary aliphatic amines, at 3354 and 3289 cm^{-1}, as broad bands due to the N–H asymmetric and symmetric vibrations, respectively. The weak peak of secondary amines (usually in the interval of 3500–3300 cm^{-1}) appears as a shoulder at 3432 cm^{-1}. An N–H bending (scissoring) vibration is observed at 1659 cm^{-1} and at 1597 cm^{-1} for primary and secondary amines, respectively, and the C–N stretching vibration is present in the 1355–1053 cm^{-1} interval.[40]

The FTIR spectrum of the cD_4^H–AGE–PEI conjugate reveals the strong peaks of primary and secondary amines slightly shifted to 1666 cm^{-1} and 1599 cm^{-1}, respectively, and the medium absorption bands in the region 1350–1058 cm^{-1} due to the C–N bond of primary, secondary, and tertiary aliphatic amines of PEI moieties, which are superposed with Si–CH$_3$ and Si–O specific bands. The strong bands at 2939 cm^{-1}, 2821 cm^{-1} and 1457 cm^{-1} are attributed to the C–H stretching and rocking vibrations of PEI and cD_4^H–AGE moieties.

The wide scan XPS spectrum of cD_4^H–AGE–PEI allows the determination of the elemental composition of the conjugate carrier, and consequently the calculation of the recipe to produce polyplexes between the carrier and DNA, in order to ensure the obtaining of precise N/P ratios, as required to correctly estimate the transfection efficacy. The peaks of binding energies of 99, 150, 283, 396 and 529 eV were assigned to Si 2p, Si 2s, C 1s, N 1s and O 1s, as Fig. S2 (in ESI†) depicts. Table 1 summarizes the elemental concentrations, which confirm the postulated structure of the conjugate.

Table 1 Atomic and mass concentrations calculated from XPS wide spectra of PEI and cD_4^H–AGE–PEI

	Assignment							
	O		N		C		Si	
Sample	Atomic conc. (%)	Mass conc. (%)	Atomic conc. (%)	Mass conc. (%)	Atomic conc. (%)	Mass conc. (%)	Atomic conc. (%)	Mass conc. (%)
PEI			34.44	37.99	65.56	62.01		
D4–AGE–PEI	7.43	9.05	24.48	26.10	65.94	60.27	2.15	4.59

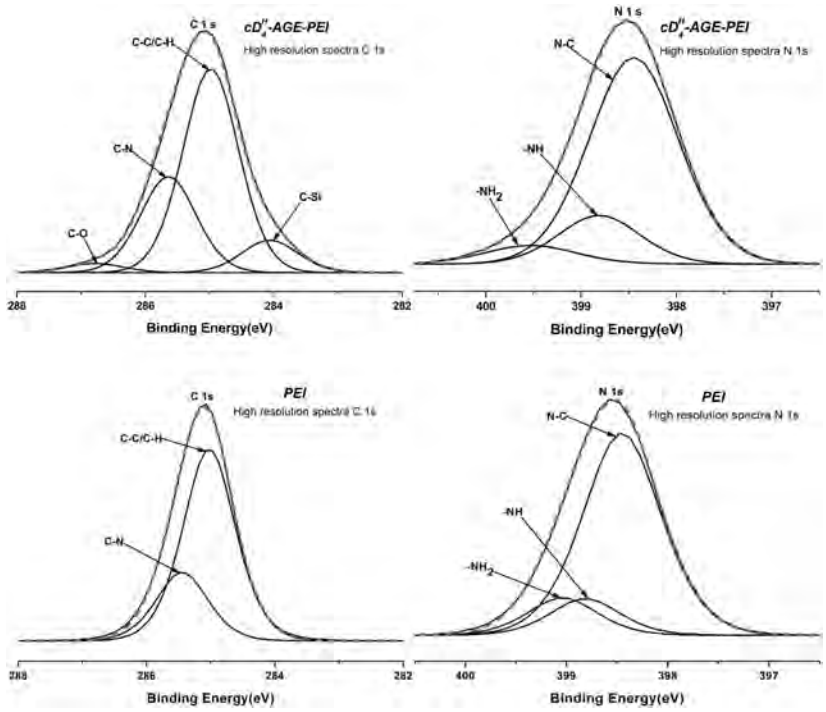

Fig. 2 Deconvolved high resolution spectra of C 1s (left column) and N 1s (right column) for PEI and the cD_4^H–AGE–PEI conjugate.

C 1s and N 1s high resolution spectra of cD_4^H–AGE–PEI (Fig. 2), along with Table S1 in the ESI,† covering assignments and concentrations of encountered chemical bonds, aimed to confirm once more the structures demonstrated by NMR and FTIR spectroscopy. The N 1s peak was resolved into three deconvolved peaks, assigned to the tertiary (═*N*–C), secondary (–H*N*–C), and primary (H_2N–C) amino groups linked to carbon atoms, in both free PEI and cD_4^H–AGE–PEI conjugates. Considering the calculated relative concentration of these chemical bonds (according to Table S1, ESI†), it is obvious that the conjugate shows different ratios between nitrogen involving bonds, as compared with free PEI, with a consequent decrease in primary amino groups in favor of secondary ones. This modification in the amino ratios of PEI linked to the siloxane core suggests that the conjugation reactions between the cD_4^H–AGE precursor and PEI occurred mainly through primary amines.

Thermogravimetric and differential scanning calorimetry analyses were performed on PEI, the cD_4^H–AGE precursor, and the cD_4^H–AGE–PEI conjugate, in order to evaluate the characteristic temperatures of the three compounds, and to validate the presence of the cyclic siloxane in the carrier molecule. Fig. S3 (ESI†) shows the TGA thermograms of the studied structures, alongside their corresponding first derivative curves (DTG). PEI almost completely decomposes, exhibiting a 1.25% mass residue at the end of the thermal degradation process (700 °C). The DTG curve indicates a three stage thermal decomposition of PEI. The first stage occurs with 8% weight loss, between 50 °C and 185 °C, by ammonia loss. The second stage occurs within the range 270–345 °C, with a weight loss of 25%, by a process of ethylamine evolution. The highest weight loss (65%) was recorded in the third thermal decomposition stage, ranging from 350 to 420 °C, being attributed to the random chain cleavage, by the formation of pyrrole and *C*-substituted ethylpyrroles.[41]

The cD_4^H–AGE precursor thermally decomposes above 260 °C in a single stage, with a mass loss of 83% and a residue value of 15%, by a mechanism of random bond cleavage. Even if it is known to be a volatile moiety (melting point of −69 °C; boiling point of 134.5 °C, at 760 mmHg), the siloxane ring remained thermally stable up to surprisingly high temperatures when entrapped in the cD_4^H–AGE molecules. Neither TGA nor DTG curves indicate evaporation phenomena below 260 °C in the case of the cD_4^H–AGE precursor. Considering that the open chain counterparts of cD_4^H possess notably higher thermal stabilities (boiling points of 165.9 °C for 3,3,5,5-tetramethyltetrasiloxane, and 172.6 °C for 1,1,3,5,7,7-hexamethyltetrasiloxane), probably the thermal scission of the cD_4^H cycle consumes increased amounts of heat, additionally biasing the thermal degradation.

The cD_4^H–AGE–PEI conjugate exhibits a similar evolution of thermal decomposition to that of PEI, in three stages, as shown by the DTG curve. The first stage (120–260 °C, 12% weight loss) emphasizes the overlapping of thermal elimination of solvent traces, and of ammonia and ethylamine evolution from PEI molecules. The process continues in the second stage (260–375 °C, 70% weight loss), in parallel with the random chain scissions of the whole polymeric structure. In contrast with PEI, the third stage of cD_4^H–AGE–PEI thermal decomposition is shifted to higher temperatures (380–445 °C), and exhibits a

significantly lower value of weight loss (10%, in comparison with 65% in the case of PEI). The same effect is revealed by the lower amplitude of the second DTG curve peak, at 415 °C. In this respect, two explanations are possible: (i) the higher number of hydrogen bonds intramolecularly established in the cD_4^H–AGE–PEI edifice, or (ii) the lower relative content of PEI in the conjugate, considering that both PEI and conjugate samples had practically the same weight. A higher value of thermostable residue was yielded by cD_4^H–AGE–PEI (7%) as compared with pure PEI (1.25%), certainly due to the siloxane content.

According to DSC analysis (Fig. S4, in ESI†), PEI shows a typical domain of glass transition temperature (T_g), centered at −57 °C. Although it is not a macromolecular compound, due to its bulky structure and to the presence of highly mobile and relatively long AGE moieties, the cD_4^H–AGE sample yields a T_g value of about −75 °C. Moreover, such a lowered T_g value is due to the presence of the cyclic siloxane moiety, which consists of highly flexible –Si–O– bonds. The second DSC heating curve of structure cD_4^H–AGE–PEI conjugate exhibits a significant increase in T_g value (−33 °C), as a consequence of the higher number of hydrogen bonds, which leads to an important steric hindering of segmental chain mobility, owing to decreased free volume in the sample.

Mass spectrometry analysis was performed in the electrospray ionization variant (ESI-MS), in order to confirm the molecular structure of the cD_4^H–AGE–PEI carrier. Formation of the molecular ion by ESI-MS occurs only in the positive mode, and therefore only positive ions were analysed. Positive ESI produces one major and several minor series of oligomer ions of 43 Da (a value which corresponds to the CH_2CH_2NH repeat unit), apart from each other.

The ESI spectrum of cD_4^H–AGE–PEI (Fig. S6, ESI†) reveals the presence of two or more Na^+ cations attached to the conjugate molecule, thus forming multiply-charged ions. Although the molecular weight distribution is shifted to lower masses (350–1600 m/z), the presence of multiply-charged ions (2+ to 5+) confirms that the conjugate includes an average of 3.7 molecules of PEI grafted on each siloxane cycle, and suggests that the average molecular weight of cD_4^H–AGE–PEI is 7.3 kDa. Before ESI characterization of the cD_4^H–AGE–PEI carrier, its purity was verified by HPLC. Fig. S7 (ESI†) reveals a well-defined unimodal peak, demonstrating that the investigated samples were adequately purified.

The dissociation constants (the pK_as) of the naked and loaded carriers represent a measure of their ability to promote the ''proton sponge'' mechanism of escaping from the endosomal vesicles. This effect is induced by entities with a high buffering capacity.[42] The buffer index (also named buffering capacity) defined as

$$\beta = \frac{dC_a}{dpH} = \frac{dC_b}{dpH}\ (\text{mol L}^{-1}),$$

(where C_a is the concentration of added acid, and C_b is the concentration of added alkali) reaches its maximum value when pH = pK_a.[43] Therefore, starting from an accurate titration curve with a large enough number of experimental points, the pK_a values can be established based on the maxima of $\beta = f(\text{pH})$ curves. Fig. S8 (in ESI†) shows these curves plotted for the naked cD_4^H–AGE–PEI carrier, and for the cD_4^H–AGE–PEI/dsDNA polyplexes with an N/P ratio of 10. Titration with 0.1 M HCl demonstrated that both the naked and the loaded carriers have pK_{a1} values higher than 4.5, which ensures an efficient buffering action inside the endosomal vesicles (having a local pH of about 5). Therefore, the ''proton-sponge'' endosomal escape mechanisms can be promoted, delivering the vectors into the cytosol. The titration performed with dsDNA simulates the intra-endosomal equilibria between the naked and the loaded carriers. Fig. S8(c) (ESI†) evidently shows that at pH values of around 5, the mentioned equilibria are unfavorable to the loaded form.

The partition coefficient of non-ionised cD_4^H–AGE–PEI conjugate in the 1-octanol/water immiscible system, quantified by the log P value, represents a measure of its ability to cross lipid membranes. Positive values of log P indicate greater solubility in the non-aqueous phase, while negative ones indicate a predilection for aqueous milieus. Only amphiphilic molecules having moderate volumes and log P values in the range −2 to +4 can penetrate cell membranes by virtue of a passive diffusion mechanism (not involving endocytosis or vectorized transport), while those having larger negative values are strongly repelled, and those with larger positive values are sequestered into the lipid layers.[44] The log P value experimentally determined for the cD_4^H–AGE–PEI conjugate was −1.902 ± 0.06, which defines the synthesized carrier as a molecule with moderate hydrophilicity, placed at the limit of capability to pass across lipid barriers by non-activated mechanisms. Considering the large number of protonatable amine groups of the PEI moiety, the unexpectedly low value of log P (which indicates a mass distribution ratio of about 79 : 1 between the aqueous and non-aqueous phases, when cD_4^H–AGE–PEI is in the quasi-non-protonated state, at a pH value of 10.8) could be related to some conformational peculiarities of the carrier macromolecule, like a relative space segregation of the hydrophilic and hydrophobic domains, which do not mutually hinder each other. To confirm this assumption, the conformation of cD_4^H–AGE–PEI was studied by computational chemistry techniques.

The *in silico* determined conformation and molecular dynamics of the cD_4^H–AGE–PEI conjugate

In order to reveal the ability of the cD_4^H–AGE–PEI conjugate to ionically interact with the DNA molecule, its conformation and dynamic behavior in the aqueous milieu, at physiological pH, were investigated by computational techniques. As a first step, the PM3 semiempirical molecular orbital calculations were performed to optimize the conjugate geometry *in vacuo*. Fig. S5 (in ESI†) depicts the resulting conformation, which emphasizes an asymmetric structure, with a tendency to distinctly expose the charged (PEI segments) and the uncharged (the siloxane ring and the linker AGE moiety) domains. According to PM3 calculations, the cD_4^H–AGE–PEI macromolecule belongs to C_1 molecular point group symmetry. A heat of formation of

−1029.2 kcal mol^{-1}, a maximum length of 35.746 Å, a molecular volume of 7187 Å^3, a polarizability volume of 329.36 Å^3, a solvent accessible surface area of 2480 Å^2, and an appreciable dipole moment of 8.30 Debye are the main characteristics of the *in vacuo* optimized conformation of the carrier.

The dynamics simulations of the interaction between the cD$_4^H$–AGE–PEI carrier and the DNA double-helix were performed using the YASARA program suite, which is targeted on (bio)organic molecules, but does not allow automatic parameterization for inorganic atoms such as silicon. This is why the force field parameters of the carriers were generated by the AutoSMILES algorithm considering the siloxane ring in the frozen state at the level of the previously developed PM3 model (using the fixed atoms option, as suggested by YASARA developers).

According to the simulation protocol, the macromolecules (DNA and cD$_4^H$–AGE–PEI) were solvated in the entourage of 32 823 TIP3P water molecules, in a rectangular box of size 100 Å × 100 Å × 100 Å. The periodic boundary conditions were set for the simulating box. The system summing up 99 783 atoms was initially equilibrated by energy minimization simulation, using the steepest descent algorithm followed by the simulated annealing minimization.

The molecular dynamics simulation was carried out using the self-parameterizing knowledge-based YASARA force field.[45,46] For the production run, the pressure control was enabled by setting the solvent probe mode, *i.e.* water density of 0.997 g cm^{-3}, that corresponds to the conditions of a constant pressure of 1 bar, and a temperature of T = 298 K. A time step of 1 fs was applied to integrate the equations of motion. For calculating the non-bonding interactions (van der Waals and electrostatic), a cut-off distance of 12 Å was used. The electrostatic interactions have been computed by the particle mesh Ewald (PME) method. Finally, a 10 ns long molecular dynamics simulation was started and the snapshots were recorded.

Fig. 3 shows selected snapshots from the molecular dynamics computation, depicting the interaction between DNA and the polycationic cD$_4^H$–AGE–PEI molecule, *versus* the simulation time. As shown in Fig. 3a, at the initial time (t = 0), DNA and the carrier are separated by a distance of 30.5 Å between their centers of geometries (COG distance). At the simulation time of t = 2 ns, the intermolecular COG distance becomes shorter, *i.e.* 14.32 Å, and the formation of the polyplex structure can be clearly observed (Fig. 3b). For higher values of simulation time, the polyplex structure between DNA and cD$_4^H$–AGE–PEI is stabilized as shown in Fig. 3c (for t = 6 ns) and Fig. 3d (for t = 10 ns).

The most relevant molecular dynamics simulation results are summarized in Table S2 (in ESI†). According to the dynamics computation, the total potential energy E_p of the system has greatly decreased from its initial value, suggesting that the formation of the polyplex aggregate is an energetically favorable process.

As the intermolecular COG distance between DNA and cD$_4^H$–AGE–PEI decreases, the number of atoms in the

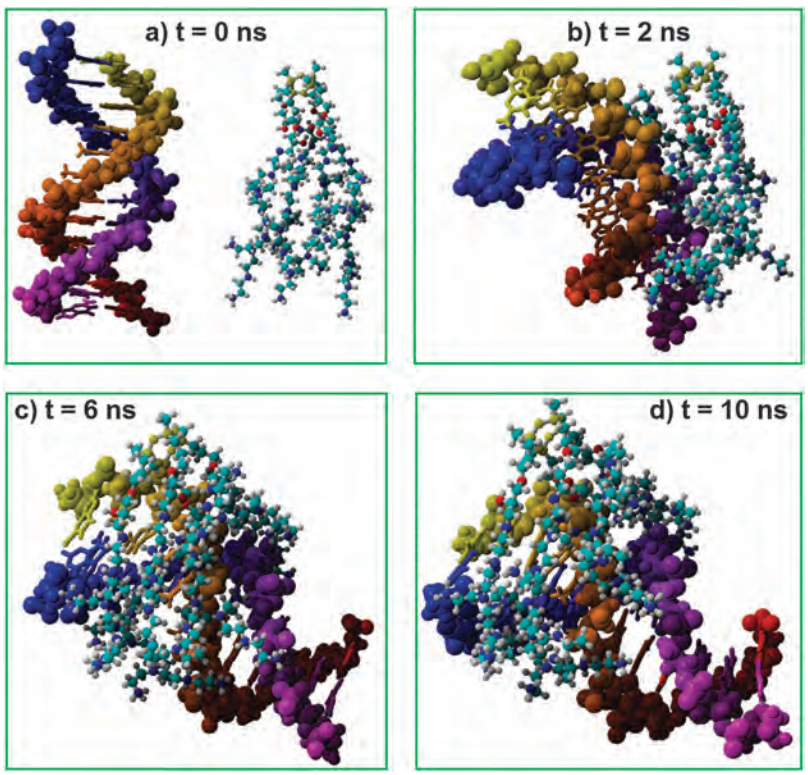

Fig. 3 Snapshots from trajectory showing the interactions between DNA and the cD$_4^H$–AGE–PEI carrier, indicating the polyplex formation at different simulation times: (a) t = 0 ns; (b) t = 2 ns; (c) t = 6 ns; (d) t = 10 ns (water molecules are omitted).

intermolecular contact (for a cutoff radius lower than 4 Å) increases significantly. As an example, at t = 2 ns the number of atoms in contact increases from zero to 387. For simulation time values greater than 4 ns, the number of atoms in the intermolecular contact varies between 500 and 611. The close contact between DNA and the cD_4^H–AGE–PEI carrier leads to the formation of hydrogen bonds, which stabilize the polyplex structure. For a simulation time t > 4 ns, the number of hydrogen bonds is higher than 8 and the corresponding total energy of the hydrogen bonds is greater than 40 kcal mol^{-1}. The hydrogen bonds are formed between the amino groups of PEI chains of the carrier and the DNA backbone oxygen atoms (*i.e.* mainly with O 1p and O 2p, and sporadically with O3*).

A widely used measure for the characterization of the conformation of a macromolecule is the radius of gyration (R_g), which measures the root-mean-square distance of the collection of segments from their common center of mass. During molecular dynamics computation, the radius of gyration of DNA has slightly fluctuated in the narrow range 13.41 to 13.77 Å. By contrast, the radius of gyration of the cD_4^H–AGE–PEI molecule has increased from 10.42 Å to a maximum value of 11.22 Å. To facilitate the structural comparison of each conformation during molecular dynamics, the root mean square deviation (RMSD) of atomic positions[47] was calculated for each pair of structures (*i.e.* initial structure *versus* relaxed structures at different times). When the RMSD value is higher than 3 Å, the structures are considered to be unlike (distinct).[48] In our study, the RMSD values for DNA among relaxed structures ranged between 1.87 Å and 2.28 Å (see Table S2, in ESI†), suggesting that all relaxed structures are quite similar to the initial equilibrated structure given by energy minimization. In other words, the DNA molecule does not suffer conformational alteration during the interaction with the carrier. On the contrary, in the case of cD_4^H–AGE–PEI the RMSD is higher than 7 Å, indicating that the relaxed conformations are different from the initial structure. Both the radius of gyration and the RMSD values revealed a stable conformation of the DNA dodecamer. This may be attributed to the short length of the strands and hydrogen bonds between base pairs that maintain the DNA stability. In contrast, the same parameters for the carrier suggest that its macromolecule is very flexible.

The obtaining and investigation of cD_4^H–AGE–PEI/pDNA polyplexes

Polyplexes were prepared by electrostatic co-precipitation between the synthesized carrier (cD_4^H–AGE–PEI) and a plasmid (pEYFP), which embed the reporter gene that controls the expression of a brighter variant of green fluorescent protein. In order to evaluate their performances, the resulting complexes were then used in transfection tests, performed in comparison with polyplexes generated using naked branched PEI, and standard SuperFect® (from Qiagen), a commercially available carrier of the activated-dendrimer type.[49] SuperFect® consists of a mixture of fragments of partially solvolyzed sixth-generation TAEA–core PAMAM dendrimers (TAEA: tris(2-aminoethyl)amine; PAMAM: polyamidoamine),[50,51] and it is widely used in practice as a polymeric transfection agent. Its efficacy is considered to originate in the increased flexibility of the fractured dendrimer molecule,[52] which enables a tighter intimate association with DNA.

The recipes to prepare the cD_4^H–AGE–PEI-based, PEI-based and SuperFect-based polyplexes were identical. The liquid phase of the samples consists of a TAE buffer at pH 7.4, the amount of DNA was kept constant (1 μg for each 20 μL sample solution), and the amount of carrier was calculated in order to obtain the imposed N/P molar ratios. As an example, to prepare cD_4^H–AGE–PEI/pEYFP polyplexes having a N/P molar ratio of 1, 1 μg plasmid (10 μL of a stock solution of 1 mg plasmid dissolved in 10 mL 1× TAE buffer) was mixed with 0.161 μg of synthesized conjugate (10 μL of a ten-fold diluted stock solution of 1.61 mg carrier dissolved in 10 mL 1× TAE buffer), keeping in mind that 1 μg DNA contains 3 nmol phosphate groups, and that cD_4^H–AGE–PEI contains 26.1% w/w nitrogen. After mixing the solutions of the two components, the resulting 20 μL samples were carefully vortexed, and then maintained at room temperature for one hour. Applying the same procedure, polyplex samples were prepared using pEYFP and 2 kDa and 25 kDa PEI.

Determination of polyplex ζ-potential. The colloidal stability of the prepared polyplexes was investigated by measuring the dependence of their zeta potential on the N/P ratios, at two different pH values, 7.4 (specific to the arterial blood) and 5.5 (a common value in endo- and lysosomes), buffered by TAE (Tris-acetate–EDTA) mixtures, with and without ionic strength correction (by using NaCl). To ensure an elevated level of transfection efficacy, polyplexes need to comprise a small excess of positive charges, able to prevent colloidal aggregation, especially in aqueous systems with salt content.[53] Such an excess of charges was evidenced for the cD_4^H–AGE–PEI/pEYFP polyplexes, as depicted in Fig. 4. Values of zeta potential of about 10 mV or greater seem to be favorable, and were measured for N/P ratios above 30, regardless of the pH and ionic strength.

The nanoparticulate size and morphology of cD_4^H–AGE–PEI/pEYFP polyplexes was evidenced by AFM, in relation to the

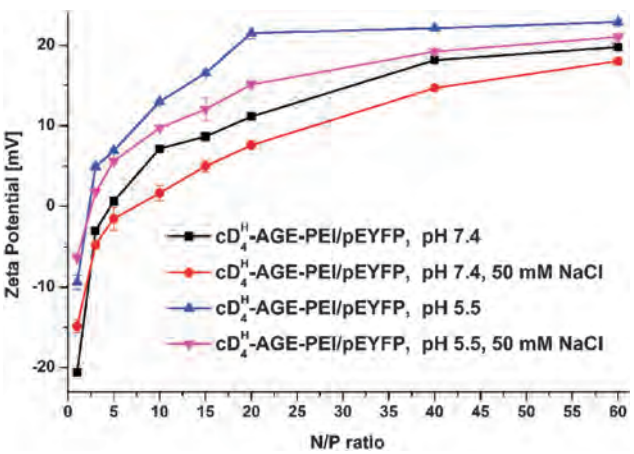

Fig. 4 Evolution of zeta potential of cD_4^H–AGE–PEI/pEYFP polyplexes prepared at different N/P molar ratios, in buffered aqueous milieus.

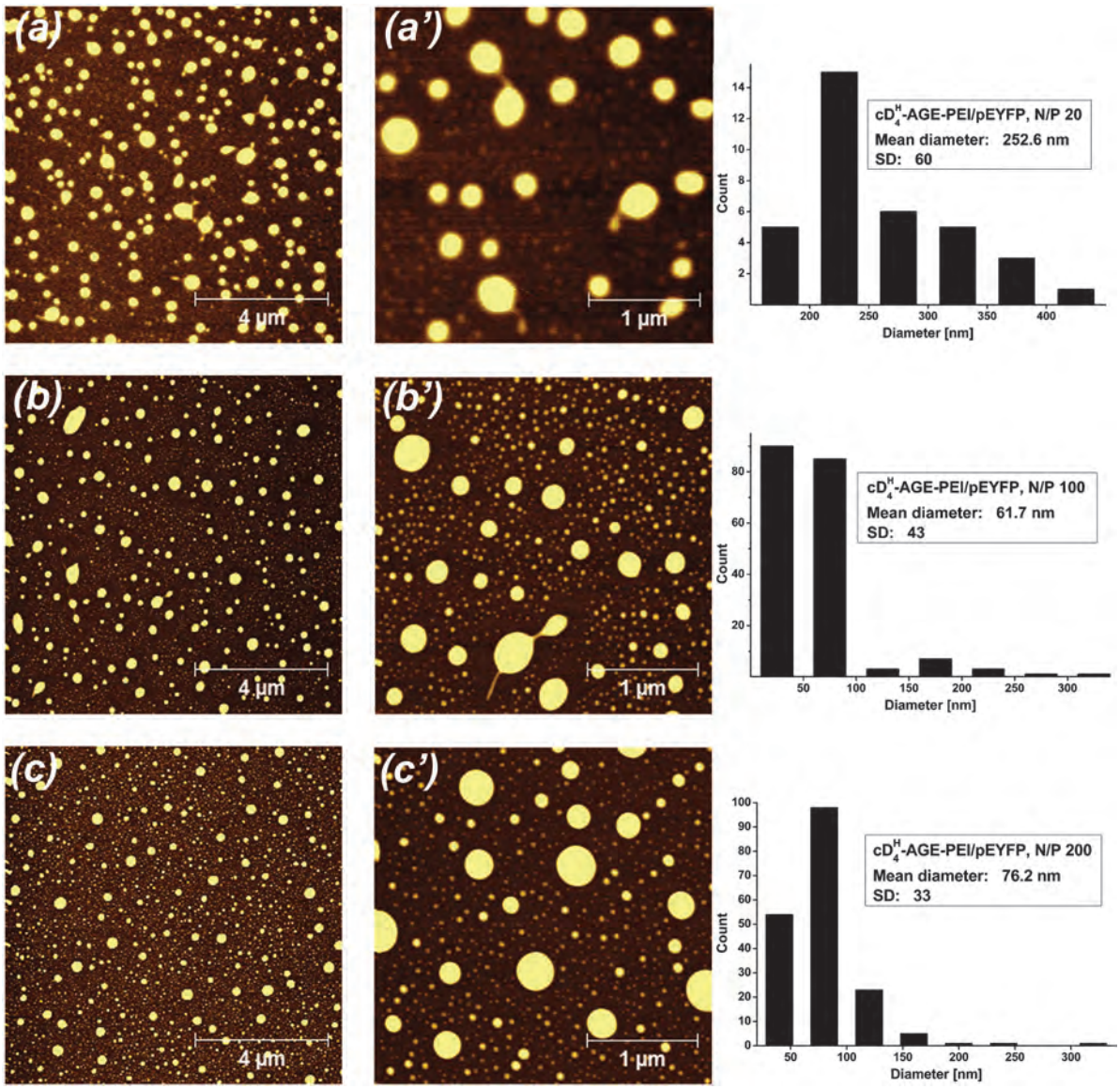

Fig. 5 AFM imaging of cD_4^H–AGE–PEI/pEYFP polyplexes, evidencing their morphology and dimensional distribution at three values of N/P ratio, as measured at pH 7.4 (TAE buffer), without NaCl addition.

composition of carrier-pDNA aggregates. Fig. 5 presents the AFM results obtained for three values of N/P ratios. In all cases the resulting particles are spheroidal and well individualized. A narrower unimodal distribution of nanoscale particles was evidenced for polyplexes having a N/P ratio of 200. At the smallest investigated N/P ratio (of 20), the polyplex particles have average diameters outside the nano-range, while at the central N/P value (of 100) the dimensional distribution is located below 100 nm, but the dispersion of the values is somehow monotonic. Such a dimensional variation with the N/P ratio may be only partially correlated with the zeta potential of the polyplex particles, at pH 7.4.

Gel retardation assay. The ability of the cD_4^H–AGE–PEI carrier to fully and firmly associate with plasmid DNA was tested by the gel retardation assay (also known as "electrophoretic mobility shift assay" – EMSA). During the agarose gel electrophoresis performed at a pH value of 7.4, the negatively-charged pDNA molecules tend to migrate towards the anode. As a consequence of the association with the positively-charged carriers, the migration is delayed to an extent that depends on the molar ratios between the interacting charges, and on the dimensions of the resulting aggregates. Migration ceases when a stoichiometric electrostatic interaction occurs between the molecules of pDNA and of the carrier, and is completely inhibited when the positive charge of polyplexes prevails. Based on this mechanism, one can establish the limited value of the N/P ratio, which promotes a stable complexation, and the range of mixing amounts, that favor the transfection of pDNA mediated by the investigated carriers. Fig. 6 presents the results of gel retardation assay

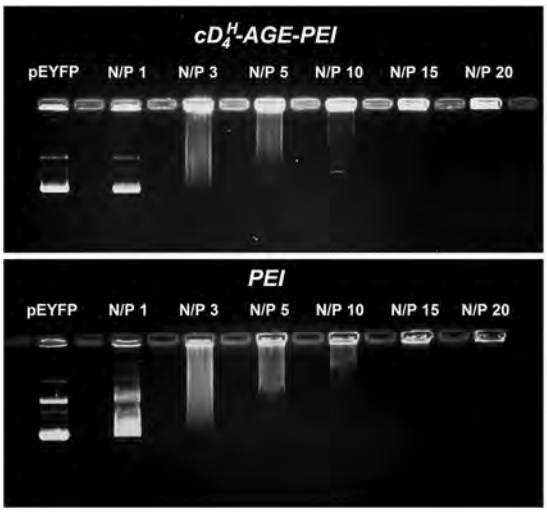

Fig. 6 Electrophoretic migration of cD_4^H–AGE–PEI/pEYFP (a) and PEI/pEYFP (b) polyplexes having N/P ratios of 1, 3, 5, 10, 15 and 20, in comparison with the migration of free plasmid.

applied to PEI/pEYFP and cD_4^H–AGE–PEI/pEYFP polyplexes. It is obvious that the plasmid migration is completely suspended at N/P ratios higher than 10, in the cases of both free 2 kDa PEI and of the conjugate carrier. Possible small differences could be generated (for N/P ratios in between 10 and 15) by the molar fraction of charged atoms in the molecular structure.

***In vitro* cytotoxicity assay.** The potential cytotoxicity of the cD_4^H–AGE–PEI conjugate carrier was tested in parallel with that of free PEI, both for the unloaded form and for polyplexes with pEYFP. The viability of HEK 293T cells cultured in the presence of unloaded carriers and polyplexes was measured using the MTT technique. In order to obtain scalable data, the dosed amounts of unloaded carriers were identical with the corresponding weight amounts used to prepare polyplexes with defined N/P ratios. Fig. 7 presents the calculated cell viability, expressed as an average percentage relative to the control culture (considered 100%), and based on three parallel experiments. No significant difference could be observed in cellular viability after 48 hours incubation in the presence of uncomplexed cD_4^H–AGE–PEI and complexed cD_4^H–AGE–PEI/pEYFP, at any of the tested N/P ratios. For N/P ratios of up to 20, the viability of HEK 293T cells is not affected, but a slight decrease was observed at higher values (about 90% at N/Ps of 30 and 60, and about 80% at higher N/Ps). These results point out the cytocompatibility of cD_4^H–AGE–PEI/pEYFP polyplexes, which are applicable even for N/P ratios greater than 100. A quasi-similar evolution of cytocompatibility was noticed in the case of free and complexed PEI, up to N/P ratios of 150. At higher values, 2 kDa PEI induces an unacceptable decrease of cellular viability, of about 30% as compared with the control culture.

To evaluate the blood compatibility of PEI/pEYFP and cD_4^H–AGE–PEI/pEYFP polyplexes after intravenous administration, the induced hemolysis and erythrocyte aggregation were

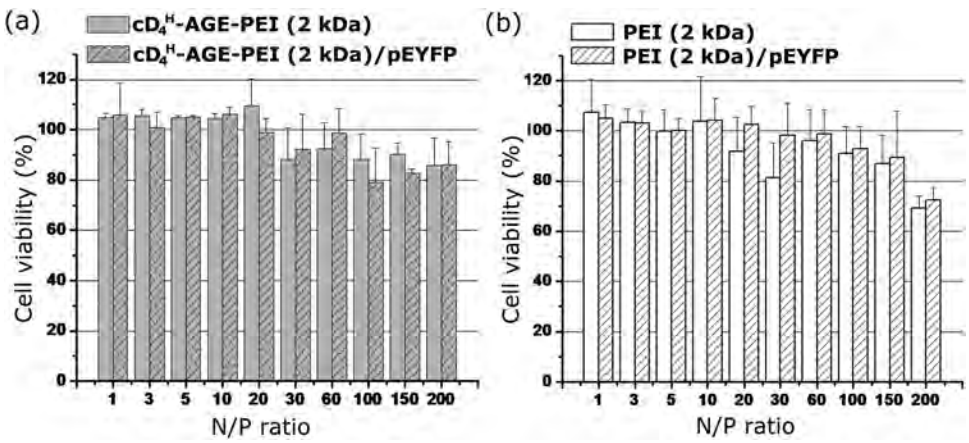

Fig. 7 *In vitro* cytotoxicity assay using MTT method. Relative viabilities of HEK 293T cells after incubation with cD_4^H–AGL–PEI (2 kDa) (a) and PEI (2 kDa) (b), both in unloaded form or complexed with pEYFP plasmid at different N/P ratios. The results are presented as mean ± standard error from 3 independent experiments performed in triplicate.

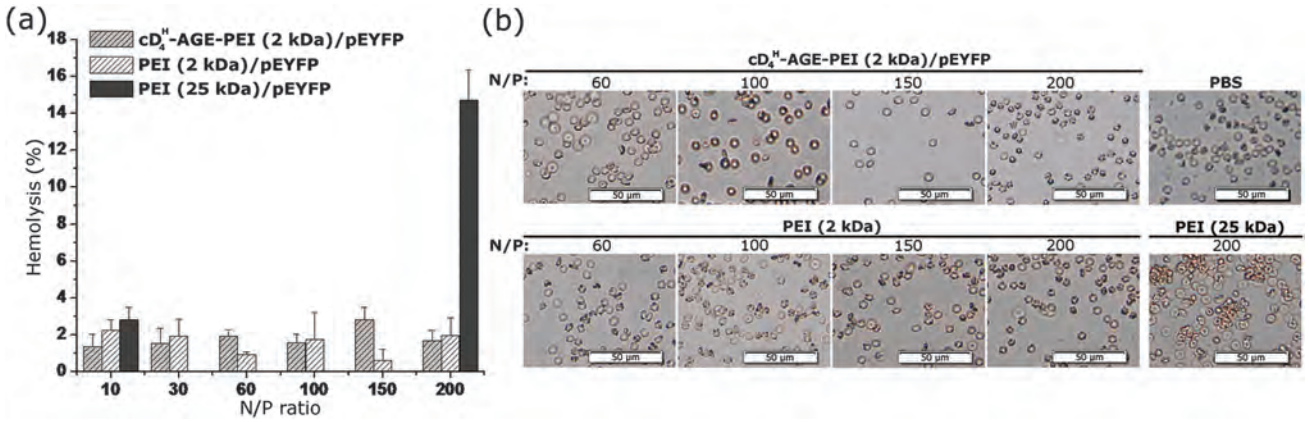

Fig. 8 (a) Percentage of hemolysis induced by 2 kDa PEI/pEYFP and cD_4^H–AGE–PEI/pEYFP polyplexes, compared with the hemolysis generated using 25 kDa PEI, at different N/P ratios. (b) Evaluation of erythrocyte aggregation after the treatment with the same investigated polyplexes, and PBS (negative control). Scale bar: 50 μm.

investigated. The 25 kDa PEI was used as the blood toxicity reference compound. Polyplexes having N/P ratios of 10, 30, 60, 100, 150 and 200 were studied, and for the extreme values in this series, polyplexes based on 25 kDa PEI were also tested with the aim of comparing the blood toxicity results with the values induced by a known to be toxic compound. Hemolysis was determined spectrophotometrically, by measuring the absorbance of the released hemoglobin, at 540 nm. Fig. 8a reveals that the hemolytic activity of cD_4^H–AGE–PEI/pEYFP polyplexes is less than 3%, even at the highest N/P ratio of 200 (which is equivalent with a dose of 28.64 mg polyplex per kg body weight of mice). Hemolysis induced by PEI/pEYFP polyplexes also ranks below 3%, regardless of the N/P ratios. In comparison, the hemolytic activities of polyplexes obtained using 25 kDa PEI were 2.8 ± 0.68% at an N/P ratio of 10, and 14.72 ± 1.63% at the maximum ratio, respectively.

The degree of erythrocyte aggregation is considered to be a measure of the potential increase in blood viscosity, under the effect of an administered (bio)chemical compound. Such an effect is able to severely restrict or even block the capillary flow. To evaluate the aggregation, the erythrocytes isolated after hemolysis assay were observed using a microscope, under bright field (Fig. 8b). The incubation with PEI/pEYFP and cD_4^H–AGE–PEI/pEYFP polyplexes, at any N/P ratio (up to 200), caused no erythrocyte aggregation, the samples behaving similarly to the negative control (incubation in PBS). In the case of 25 kDa based polyplexes, the treatment had no influence at an N/P ratio of 10 (data not shown), whereas for a ratio of 200, aggregation occurred.

The transfection efficiency of the cD_4^H–AGE–PEI carrier was calculated based on the flow cytometry data, and compared with the results obtained using 2 kDa PEI polyplexes, and 25

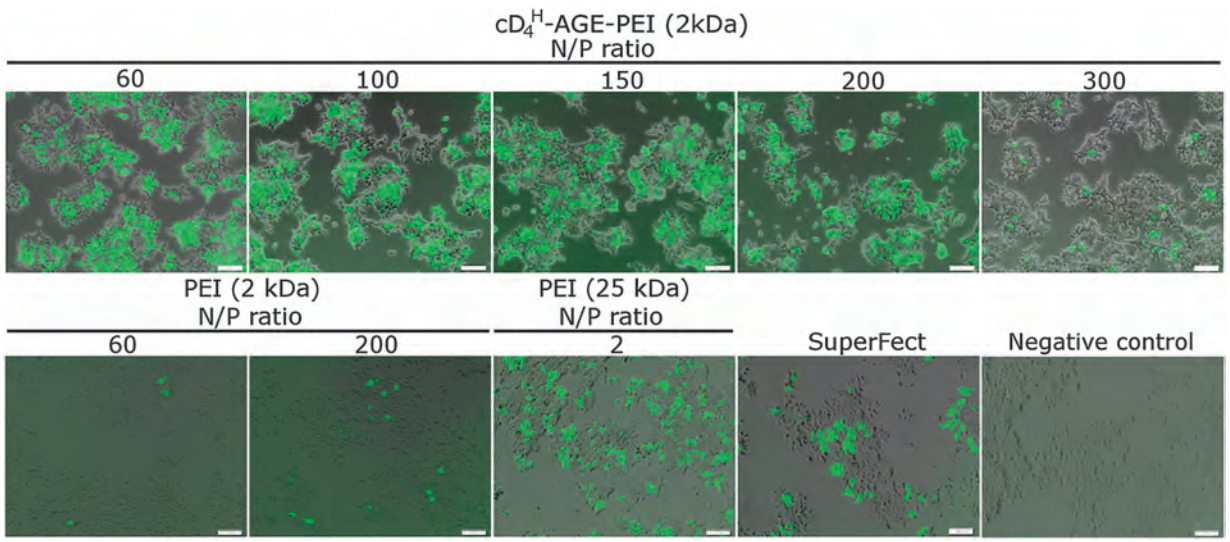

Fig. 9 Overlay of bright field and green fluorescence microscopy images showing the expression of EYFP protein in HEK 293T cells transfected with cD_4^H–AGE–PEI/pEYFP polyplexes at different N/P ratios. As controls, cells transfected with 2 kDa and 25 kDa PEI/pEYFP polyplexes, and with SuperFect® are included, alongside the negative control of untransfected cells. The scale bar indicates 100 μm.

kDa branched PEI, and the SuperFect® commercial product, all of them considered to be positive controls. The untransfected cells were taken into account as the negative control. Qualitatively, transfection results were shown by fluorescence microscopy, as presented in Fig. 9. The percentage of EYFP-positive cells and the value of mean fluorescence intensity (MFI) of transfected cells (which is a direct measure of the level of fluorescent protein transduction) were measured by flow cytometry, and are included in Fig. 10. For N/P ratios below 60, very low transfection efficiencies were obtained, both in terms of percentage of EYFP-positive cells, and of fluorescent protein expression level. At increased N/P ratios (60, 100 and 150, respectively), about 3% EYFP-positive cells, and similar levels of EYFP protein transduction could be attained. At an N/P value of 200, a statistically significant increase ($p < 0.05$) in the number of transfected cells resulted for cD_4^H–AGE–PEI/pEYFP polyplexes (a EYFP-positive cells percent of about 35%), whereas the MFI remains at the same levels as that obtained for lower N/P ratios. A dramatic decrease in the percentage of transfected cells (down to about 5%) was obtained for an N/P ratio of 300. The MFI also decreased by about 38% relative to the value measured at an N/P ratio of 200.

To investigate whether the 2 kDa PEI-based cD_4^H–AGE–PEI conjugate is superior in transfection efficiency as compared

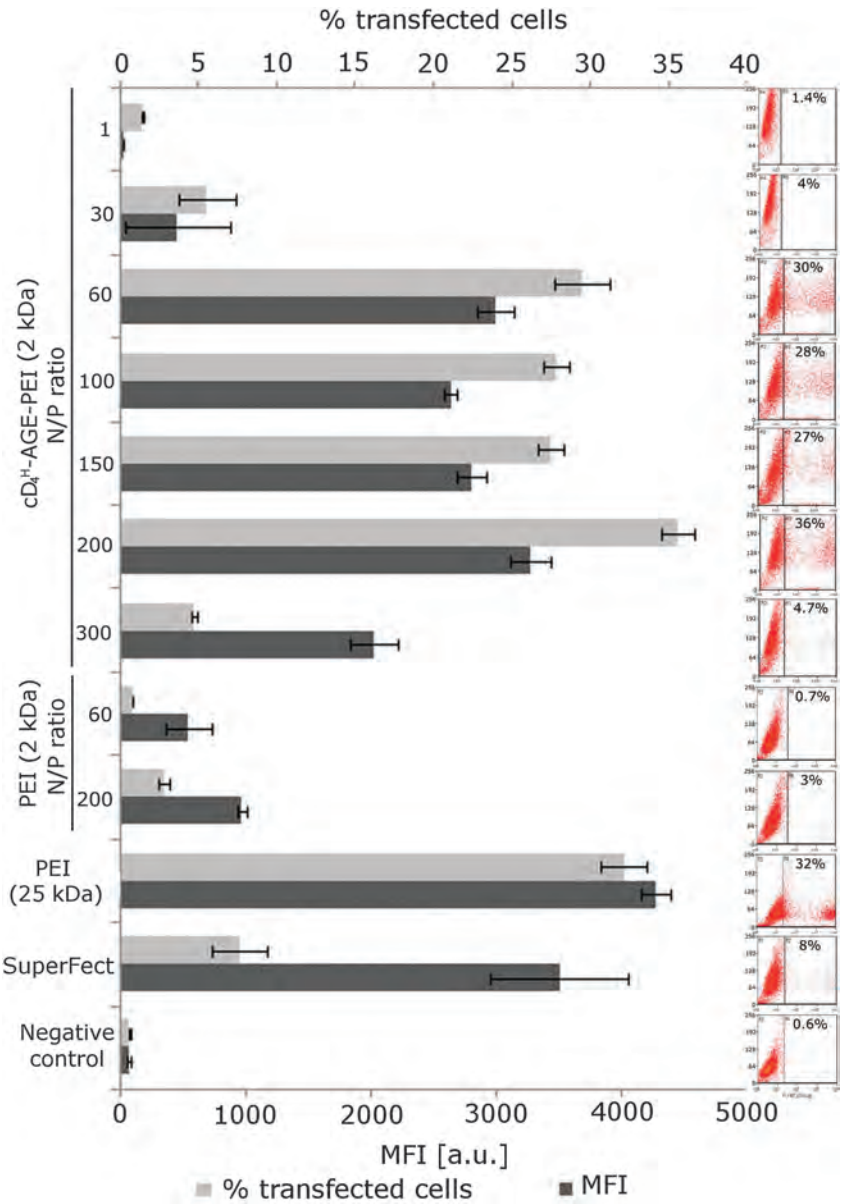

Fig. 10 The percentage of transfected cells and the mean fluorescence intensity of the cells analysed by flow cytometry. Positive (cells transfected using branched 25 kDa PEI, and with the SuperFect® commercial reagent kit) and negative (untreated cells) controls are included. Representative dot plots of flow cytometry analysis presenting side scattering (SSC) *versus* EYFP fluorescence (FL1) of transfected HEK 293T cells, and showing the percentage of EYFP-positive cells are placed in the right hand column.

with the 2 kDa free PEI carrier, their polyplexes have been tested at the same N/P ratios. The obtained transfection efficiency was about 0.7% and 3% at N/P ratios of 60 and 200, respectively. At an N/P ratio of 2, the branched 25 kDa PEI used as a positive control, showing transfection percentage values statistically similar to those obtained for cD_4^H–AGE–PEI/pEYFP polyplexes having N/P ratios between 60 and 200. Regarding the level of fluorescent protein expression, it is significantly increased (by 23%, $p = 0.0073$) when 25 kDa PEI/pEYFP polyplexes at an N/P ratio of 2 are compared with cD_4^H–AGE–PEI/pEYFP polyplexes at an N/P ratio of 200. The very low N/P ratio of 2 was chosen to test 25 kDa PEI/pEYFP polyplexes because the cellular viability at this ratio is about 80%, but significantly decreases (to less than 60%) when the N/P ratio increases to 10 (data not shown). In the case of 25 kDa PEI/pEYFP polyplexes with an N/P ratio of 10, the percentage of transfection increases to about 40%, but the MFI decreases by 72% (data not shown). Working with the SuperFect® commercial product and following the procedure recommended as optimal by Qiagen, about 8% of the transfected cells have expressed high levels of EYFP protein. This value is entirely similar to those obtained for 25 kDa PEI/pEYFP and 2 kDa PEI-based cD_4^H–AGE–PEI/pEYFP polyplexes.

Discussion

As compared with other non-viral gene vectors, polyplexes are able to generate reproducible and highly stable cargocomplexes of large dimensions, favoring the transfection of biologically significant amounts of nucleic acids, including functional genes. Usually, polyplexes are supramolecular aggregates generated in a cooperative manner, by a variable number of individual carrier macromolecules bearing cationic charges, which electrostatically interact with nucleic acids.

There are two contradictory requirements when nucleic acids are vectorized by polyplexes: (i) to firmly but reversibly associate the carriers with the cargo, exclusively by means of physical interactions developed in a maximal number of sites, and (ii) to introduce a minimal amount of alien macromolecules into the target cell. According to the first requirement, cationic macromolecules having spatially extended edifices and large numbers of localized positive charges seem to be recommended as carriers. In this approach, carriers should be flexible lengthy linear or branched polycations, capable of entwining with the relatively rigid nucleic acid macromolecules over extended domains. Such carriers bear an excess of cationic sites, and waste a large number of them. They have excessive coverage, and "suffocate" the embedded nucleic acids with positive charges. The second requirement is related to the post-transfection fate of carriers, which must be processed intracellularly. From this point of view, carriers should have small volumes, and should be capable of locally adapting to the nucleic acid conformation. Ideally, they should not completely cover or embed the cargo, but only attach to them in a minimum number of segments, in order to optimally reduce, but not eliminate, the exposure of negative charges of nucleic acids.

The constraints imposed by the second requirement dictate the design criteria of the highly efficient nucleic acid carriers. In this respect, optimal carriers should include: (i) short but flexible, possibly branched cationic "arms", (ii) local molecular segments endowed with lipid membrane penetrating abilities, of intrinsic origin (*e.g.* lipophilicity, penetrating peptide moieties, *etc.*), or temporarily induced by the transfection milieu or by the cell proximity (cell membrane targeting molecules), (iii) a sufficient level of molecular asymmetry, to be able to distinctly expose their functional parts of the edifice during the process of conformational accommodation to the local peculiarities of the nucleic acid macromolecules. The three mentioned design criteria have guided Qiagen (the producer of SuperFect® transfection reagent) to chemically degrade an already synthesized dendrimer molecule,[50] in asymmetric pieces with cationic charged "fingers" capable of palpating the DNA molecule, and to locally attach in the most favorable conformational locations. Collaboratively, several pieces of solvolyzed dendrimers ensure an increased transfection effect.

The molecular edifice we designed (cD_4^H–AGE–PEI conjugate) obeys *ab initio* the three mentioned criteria. Its demonstrated transfection efficacy originates in its ability to tightly encompass nucleic acid molecules by electrostatic interaction mediated by the short PEI branches (which wrap the local conformation of the substrate), and consequently to expose the siloxane hydrophobic moiety. A transfection favorable effect results in the virtue of the synergism between the charge compensation of the polyanionic substrate, and the increased lipophilicity of the outer added siloxane "patches". As a consequence, the repellence exerted by the cell membrane against the resulting cargocomplexes diminishes, which increases their passive penetrability (not mediated by cell membrane mechanisms) across lipidic barriers.

Due to the molecular peculiarities of the individual cD_4^H–AGE–PEI carriers (small volume, enhanced flexibility, relative amphipathicity, and the propensity to adopt asymmetric geometries), they are able to dynamically build supramolecular aggregates, and to collectively transport nucleic acids into cells. Due to the length of PEI molecular segments, electrostatic interaction cannot be accurately punctual (in a 1:1 ratio between the amine groups of the carrier and the phosphate groups of the cargo). This is why optimal transfection is induced by the cD_4^H–AGE–PEI conjugate at N/P ratios of the order of tenths. A further refining of the transfection protocols, in parallel with the use of shorter PEI segments, could decrease the N/P of efficacious cargocomplexes.

Experimental

Materials

Allyl glycidyl ether (1-allyloxy-2,3-epoxypropane, AGL), branched low mass polyethylene imine of M_w 2000 Da (PEI), 0.1 M, platinum(0)-1,3-divinyl-1,1,3,3-tetramethyldisiloxane

complex solution in xylene (Karstedt's catalyst used in hydrosilylation reaction), dimethyl sulfoxide (DMSO), 3-[4,5-dimethylthiazol-2-yl]-2,5-diphenyltetrazolium bromide (MTT), and Tris-phosphate–EDTA buffer 10× (for gel electrophoresis) were purchased from Sigma Aldrich. 2,4,6,8-Tetramethylcyclotetrasiloxane (cD_4^H) 99% was purchased from Alfa Aesar. TAE buffer (10×) for molecular biology was purchased from ITW-AppliChem GmbH, Germany. The pEYFP plasmid was purchased from Clontech Laboratories Inc. (Mountain View, CA, USA), and the Plasmid Midi Kit from Qiagen (Düsseldorf, Germany). Dulbecco's modified Eagle's medium (DMEM), fetal calf serum (FCS), penicillin G, neomycin and streptomycin were purchased from Gibco BRL (Gaithersburg, MD, USA), and the cell culture plates were purchased from Corning (New York, NY, USA). HEK 293T cells (Human Embryonic Kidney 293T cell line) were obtained as a kind gift from Professor Dimitris Kardassis, University of Crete, Greece.

Chemical syntheses

Scheme 1 summarizes the steps involved in obtaining the siloxane-core based carrier. Further, the synthesis procedures are described in detail.

Synthesis of 2,4,6,8-tetra(3-glycidoxypropyl)-2,4,6,8-tetramethylcyclotetrasiloxane (cD_4^H–AGE)

The hydrosililation of allyl glycidyl ether (AGE) with tetramethylcyclotetrasiloxane (cD_4^H) was conducted according a modified method, originally described in ref. 38. A solution of 1.0099 g (4.2 mmol) cD_4^H in 50 mL toluene, prepared under nitrogen atmosphere, was introduced into a three-necked flask, equipped with an additional funnel and argon inlet. After careful heating of the solution to 40 °C, 70 μL of Karstedt's catalyst solution (2% in xylene) was added, and the mixture was maintained under vigorous stirring for 30 min, before adding the allyl compound (AGE). To ensure a molar ratio of 1 : 4.25 between cD_4^H and AGE, 2.0349 g (17.85 mmol) AGE was dissolved in 35 mL toluene, and then the solution was added drop-wise, through the funnel, into the reaction vessel. The progress of the reaction was monitored by FT-IR spectroscopy, observing the disappearance of the strong silicone hydride stretching band (Si–H) at 2175.62 cm^{-1}. After about 72 h, the reaction product was recovered by solvent evaporation under vacuum, as a yellow-brown liquid, in a yield of 98%. The reaction completion was confirmed by the disappearance of the Si–H bond at 4.86 ppm in the ^1H NMR spectrum.

cD_4^H–AGE. ^1H-NMR (D_2O, 400 MHz): 0.16 (bs, CH_3-1), 0.61 (bs, CH_2-2), 1.66 (bs, CH_2-3), 2.54 (bs, CH_2^A-7) and 2.71–2.73 (m, CH_2^B-7), 3.08 (CH-6), 3.29–3.33 (m, CH_2^A-5), 3.47 (bs, CH_2-4), 3.67–3.70 (m, CH_2^B-5). ^{13}C-NMR (D_2O, 100 MHz): −0.83 (CH_3-1), 13.08 (CH_2-2), 23.25 (CH_2-3), 43.46 (CH_2-7), 50.56 (CH_2-6), 71.60 (CH_2-5), 73.43 (CH_2-4).

Synthesis of the carrier molecular edifice, by the reaction of cD_4^H–AGE with PEI

At a molar ratio of 1 : 4, 0.65 g cD_4^H–AGE product, and 7.46 g PEI were dissolved in 50 mL DMSO, and heated to 80 °C, under magnetic stirring, and then 300 μL isopropanol was added (to ensure a 1 : 1 molar ratio between the alcohol and PEI). The reaction mixture was continuously stirred, at 80 °C, over a period of 40 hours. After DMSO removal by evaporation under vacuum, the reaction product was purified by dialysis against distilled water, for 7 days, using a membrane with a MWCO of 2000 (SpectrumLab, Inc.), in order to eliminate unreacted PEI, the catalyst molecules, and the accidental impurities. The final product (cD_4^H–AGE–PEI) was recovered as a yellow-brownish viscous liquid, in a 75% yield.

PEI. ^1H-NMR (D_2O, 400 MHz): 2.58 (CH_2-a), 2.59 (CH_2-b), 2.64 (CH_2-c, CH_2-d), 2.69 (CH_2-e, CH_2-f), 2.70 (CH_2-g), 2.72 (CH_2-h). ^{13}C-NMR (D_2O, 100 MHz): 37.88 (CH_2-h), 39.92 and 39.97 (CH_2-g), 45.68 (CH_2-f), 47.77 (CH_2-e), 50.67 and 50.81 (CH_2-d), 51.16 (CH_2-c), 53.20 (CH_2-b), 56.10 and 56.21 (CH_2-a).

cD_4^H–AGE–PEI. ^1H-NMR (D_2O, 400 MHz): 0.09–0.13 (m, CH_3-1), 0.57–0.58 (m, CH_2-2), 1.63 (bs, CH_2-3), 2.55 (m, CH_2-7), 2.56 (CH_2-a), 2.60 (CH_2-b), 2.66 (CH_2-c, CH_2-d), 2.68 (CH_2-e, CH_2-f), 2.70 (CH_2-g), 2.72 (CH_2-h), 3.43–3.45 (m, CH_2-5), 3.49 (bs, CH_2-4), 3.88 (CH-6). ^{13}C-NMR (D_2O, 100 MHz): −2.62 (CH_3-1), 11.70 (CH_2-2), 22.35 (CH_2-3), 37.89 (CH_2-7) and (CH_2-h), 39.97 (CH_2-g), 45.71 (CH_2-f), 47.76 (CH_2-e), 50.68 and 50.81 (CH_2-d), 51.15 (CH_2-c), 53.20 (CH_2-b), 56.09 and 56.19 (CH_2-a), 68.69 (CH_2-6), 72.80 (CH_2-5), 73.77 (CH_2-4).

The obtaining of PEI/pEYFP, and cD_4^H–AGE–PEI/pEYFP polyplexes

The polyplexes with the plasmid DNA (pDNA) were prepared at different molar ratios (N/P), considering the content of nitrogen of free PEI and of cD_4^H–AGE–PEI conjugate, and the content of phosphate groups of pDNA, according to a procedure previously described.[54] It was considered that 1 μg of pDNA contains 3 nmol of phosphate,[55] and the nitrogen contents of PEI and of cD_4^H–AGE–PEI conjugate were determined by elemental analysis, using XPS data (as described in the next section). Stock solutions of 0.5 g L^{-1} PEI and cD_4^H–AGE–PEI were prepared in 1× TAE buffer solutions of pH 5.5 and 7.4, respectively. Appropriate amounts of PEI and cD_4^H–AGE–PEI solutions were mixed, by carefully vortexing, with aqueous solutions of pDNA of known concentration, in order to obtain the prescribed N/P ratios of 1, 3, 5, 10, 15, 20, 30, 60, 100, 150, 200 and 300. After 60 minutes of incubation at room temperature, the resulting polyplexes were subjected to further physicochemical analysis, and their transfection efficiency was measured.

FTIR spectroscopy. FTIR spectra were recorded using a Bruker Vertex 70 FT-IR spectrometer, in transmission mode, at room temperature, with a resolution of 2 cm^{-1} and 32 scans. The samples were incorporated in dry KBr pellets.

NMR spectroscopy. ^1H-NMR and ^{13}C-NMR spectra have been recorded on a Bruker Avance DRX 400 spectrometer, operating

at 400.1 and 100.6 MHz for ^{1}H and ^{13}C nuclei, respectively, at 25 °C. 1D NMR signal assignments were carried out based on 2D NMR homo- and heteronuclear correlations. ^{1}H–^{1}H-COSY, ^{1}H–^{13}C-HSQC and ^{1}H–^{13}C-HMBC experiments were recorded using standard pulse sequences, in the version with *z*-gradients, as delivered by Bruker with TopSpin 1.3 PL10 spectrometer control and processing software. The spectra were recorded on a 5 mm multinuclear direct detection, *z*-gradient. All samples were dissolved in D_2O, the chemical shifts being reported to the residual solvent peak (^{1}H: 4.80 ppm).

X-ray photoelectron spectroscopy (XPS). XPS analyses were performed on a KRATOS Axis Nova (Kratos Analytical, Manchester, United Kingdom), using Al Kα radiation, with 20 mA current and 15 kV voltage (300 W), under a base pressure of 10^{-8} to 10^{-9} Torr in the sample chamber. The incident monochromatic X-ray beam was focused on a 0.7 mm × 0.3 mm area of the sample bearing surface. XPS data fitting was performed using the Vision Processing software (Vision2 software, Version 2.2.10), using mixed Gaussian–Lorentzian curves. The linear background was subtracted before the peak areas were corrected. The binding energy of the C 1s peak was normalized to 285 eV.

Mass spectrometry (MS). MS data were obtained using an Agilent 6520 Series Accurate-Mass Quadrupole Time-of-Flight (Q-TOF) LC/MS. The liquid samples were introduced into the electrospray ion source (ESI) *via* a syringe pump at a flow-rate of 0.01 mL min^{-1}. After optimization of the Q/TOF MS parameters, they were set as follows: electrospray ionization (positive ion mode), drying gas (N_2) flow rate 6.5 L min^{-1}; drying gas temperature 325 °C; nebulizer pressure 25 psig, capillary voltage 4200 V; fragmentation voltage 200 V; the full-scan mass spectra of the investigated compounds were acquired in the *m*/*z* range 100–3000. The mass scale was calibrated using the standard calibration procedure and standard compounds provided by the manufacturer. Data were collected and processed using MassHunter Workstation Software Data Acquisition for 6200/6500 Series, version B.01.03.

The HPLC analyses were carried out using a Perkin Elmer HPLC system with a Flexar Quaternary LC Pump, a Flexar LC Autosampler, a Flexar UV-vis and Refractive Index LC Detectors. A Zorbax SB C18 (5 μm, 150 mm × 4.6 mm) column was used. The temperature was kept at 35 °C. The mobile phase was a mixture of 10 : 90 v/v water and methanol HPLC grade. The flow was 1 mL min^{-1}, and the injection volume was 20 μL.

Thermal analysis. Thermogravimetric analysis (TGA) experiments were conducted on a STA 449 F1 Jupiter device (Netzsch, Germany). Approximately 10 mg of each sample was heated in an open alumina crucible, in nitrogen atmosphere, at a flow rate of 50 mL min^{-1}. A heating rate of 10 °C min^{-1} was applied. Samples were heated in the range 30–700 °C. Differential scanning calorimetry (DSC) measurements were conducted on a DSC 200 F3 Maia device (Netzsch, Germany), on samples of 10 mg, which were heated in pierced and sealed aluminum crucibles. A heating rate of 10 °C min^{-1} was applied. Nitrogen purge gas was used as an inert atmosphere, at a flow rate of 50 mL min^{-1}. The device was temperature and sensitivity calibrated with indium, according to standard procedures.

Atomic force microscopy (AFM) was used to investigate the morphology of polyplexes, on an Ntegra Spectra instrument (NT-MDT, Russia) operated in tapping mode, under ambient conditions. Silicon cantilever tips (NSG 10) with a resonance frequency of 140–390 kHz, a force constant of 5.5–22.5 N m^{-1} and a tip curvature radius of 10 nm were used. Samples were prepared by depositing 10 μL of polyplex solutions on freshly cleaved mica substrates, which where rinsed with water to remove buffer salts, and dried in air, at room temperature. Mean diameter values and size distribution of polyplexes were established by measuring the particle diameter using the ImageJ 1.48r software application, an image processing program developed by the National Institute of Health.

Determination of polyplex zeta (ζ) potential. The ζ-potential measurements were performed by using a DelsaNano C Submicron Particle Size Analyzer (Beckman Coulter), equipped with dual 30 mW laser diodes emitting at 658 nm. The instrument uses electrophoretic light scattering (ELS) to measure the ζ potential, which determines electrophoretic movement of charged particles under an applied electric field. Measurements were performed at 25 °C, and at pH 5.5 and 7.4, in triplicate. The analysis mode uses the Smoluchowski equation.

Titration of the naked and loaded cD_4^H–AGE–PEI carriers was performed potentiometrically using a 716 DMS Titrino instrument from Metrohm (Switzerland). 25 mL of cD_4^H–AGE–PEI solution, with a concentration of 1 g L^{-1} (0.14 mM) were subjected to titration using 0.1 M HCl. Each pH value was obtained after automatically adding 0.05 mL HCl, with an equilibrating time of 20 s. A volume of 25 mL solution of carrier/DNA complex was prepared starting from a 0.14 mM cD_4^H–AGE–PEI solution and the corresponding amount of salmon sperm DNA (double strands) to reach an N/P ratio of 15. The titration was performed by automatic adding of 0.05 mL 0.1 M HCl every 20 s, up to a total volume of 5 mL. The titration of cD_4^H–AGE–PEI (0.0685 mM) with salmon sperm DNA (0.035 mM) was performed under the same conditions, using 20 mL of nucleic acid solution. To determine the dissociation constants of the investigated species, the titration data were processed by numerical derivation, to obtain the dependence of the buffer index on pH values.

The partition coefficient of the cD_4^H–AGE–PEI carrier (expressed logarithmically) was determined in order to evaluate its molecular hydrophobic–hydrophilic balance, as an index of the propensity of self-aggregation in aqueous solutions, and of the ability to penetrate cell membranes. A method derived from the classical ''shake flask'' technique was used, based on the principles described in ref. 56. The aqueous phase was buffered at pH 10.8 (0.1 M borate buffer prepared in double distilled water), to bring PEI into a predominantly non-ionized state.[57] The organic phase was pure 1-octanol. Both phases were mutually saturated by shaking their mixtures of 1 : 10 v/v, for 24 hours, at room temperature (23 °C), followed by settling for 24 hours, and careful separation of the majority phase. cD_4^H–AGE–PEI was dissolved in the buffered aqueous phase

saturated with 1-octanol, at a concentration of 0.01 mol L^{-1}, considering the molecular weight of the carrier to be 7.3 kDa, as determined by mass spectrometry. The two immiscible phases were introduced, in ratios of 1 : 1, 1 : 2, and 2 : 1 v/v, to nearly full, in glass recipients with screw caps, which were then shaken for 24 hours, in a horizontal position, in a reciprocating shaker, at room temperature (23 °C). After 48 hours of free settling, aliquots were taken from the aqueous phase, and the cD_4^H–AGE–PEI was quantitated by UV-vis spectrophotometry, after complexation with copper II ions.[58] The partition coefficient was calculated, in triplicate, as the decimal logarithm of the ratio between the molar concentrations measured in the organic and aqueous phases, respectively. The average value was considered.

Agarose gel retardation assay was applied to electrophoretically evaluate the formation of the polyplexes. Both the naked pEYFP and the polyplexes obtained at different N/P ratios were mixed with loading buffer (1× TAE buffer, pH 7.4) and then loaded in a 1% agarose gel. Electrophoresis was carried out at 90 V, for 120 minutes, in TAE running buffer solution (40 mM Tris-HCl, 1% glacial acetic acid, 1 mM EDTA). The migration of free and complexed pEYFP was visualized under UV light, after staining with ethidium bromide.

Cultured cells were employed to evaluate the cytotoxicity of the carriers and the polyplexes, and to measure the polyplex transfection efficiency. The experiments were performed using HEK 293T cells (Human Embryonic Kidney 293T cell line) cultured in cell culture plates (12 or 96 wells) in Dulbecco's modified Eagle's medium (DMEM) supplemented with 10% fetal calf serum (FCS), penicillin (100 U mL^{-1}), streptomycin (100 μg mL^{-1}), neomycin (50 μg mL^{-1}), and kept at 37 °C in a 5% CO_2 incubator.

Animals. As laboratory animals, male C57BL/6 mice from Charles River Laboratories were used. All animals had access to a standard rodent diet, water *ad libitum*, and were kept at 24 °C in a temperature-controlled chamber with a 12 hour light/dark cycle. The experiments on mice had the approval of the Ethics Committee of ''Nicolae Simionescu'' Institute of Cellular Biology and Pathology, and were conducted in accordance with the EU guidelines, annexe to Directive 86/609, Appendix A, of the European Convention for the protection of vertebrate animals used for experimental and other scientific purposes (ETS no. 123, Strasbourg, 2006).

***In vitro* cytotoxicity assay.** The cytotoxicity of PEI and cD_4^H–AGE–PEI carriers, complexed or not with plasmid DNA (pDNA), was determined by measuring the viability of the HEK 293T cells after incubation with media containing the investigated molecules or aggregates, using an MTT assay. In metabolically active cells, the yellow tetrazolium salt, MTT (3-[4,5-dimethylthiazol-2-yl]-2,5-diphenyltetrazolium bromide) is reduced, by the action of mitochondrial dehydrogenase enzymes, to purple formazan that can be solubilized and quantified spectrophotometrically.[59] The assay was performed in 96-well plates following the standard procedure. HEK 293T cells were seeded at a density of 5×10^3 cells per well and kept in an incubator, at 37 °C and 5% CO_2. After 24 hours, the culture medium was replaced with one containing PEI, cD_4^H–AGE–PEI, or their polyplexes with pEYFP prepared at different N/P ratios, respectively. In all cases, an identical concentration of investigated entities was used, referred to the carrier amount. Then, after 48 hours of incubation, the culture medium from each well was removed, and the MTT solution (0.5 mg mL^{-1} in culture medium without phenol red) was added. Three hours later, the produced formazan crystals were solubilized using a lysis buffer containing 0.1 N HCl in isopropanol, for 4 hours at 37 °C. The optical absorbance of the supernatant was measured at 570 nm, with the reference wavelength at 720 nm, using a microplate reader (Tecan GENios). The results were expressed as percentages relative to the results obtained with the control cells (cells incubated in normal cell culture medium).

Blood compatibility of cD_4^H–AGE–PEI/pEYFP polyplexes was investigated by measuring the induced hemolysis and erythrocyte aggregation. Hemolysis assays were performed according to a protocol previously described.[60] Blood samples were taken from C57BL/6 mice, and treated with EDTA to prevent coagulation. Erythrocytes were separated by centrifugation at 1000*g*, for 15 minutes, at 4 °C, and the sediment was then 1 : 10 diluted with phosphate buffer saline (PBS, pH 7.4). The erythrocytes were then incubated at 37 °C, for 1 hour, in the presence of cD_4^H–AGE–PEI/pEYFP polyplexes having different N/P ratios. Incubation with phosphate PBS was used as the negative control, and incubation in water as the positive control (considered 100% hemolysis). After centrifugation of the samples (to pellet erythrocytes), the released hemoglobin was measured in supernatants, at 540 nm, using a TECAN Infinite M200Pro spectrophotometer. The pelleted erythrocytes were resuspended in PBS, placed on glass slides and examined for aggregation using an Olympus IX81 light microscope.

In vitro transfection efficiency of cD_4^H–AGE–PEI

The *in vitro* gene transfection efficiency was measured using HEK 293T cell culture, by quantifying the expression of the enhanced yellow-green variant of the Aequorea Victoria green fluorescent protein (EYFP; excitation/emission wavelengths at 513/527 nm), induced by the reporter gene carried on the pEYFP plasmid. HEK 293T cells were seeded in 12-well culture plates, at an initial density of 1.2×10^5 cells per well. After 24 hours, the culture medium was replaced by a serum-free culture medium containing PEI/pEYFP or cD_4^H–AGE–PEI/pEYFP polyplexes prepared at N/P ratios of 1, 3, 5, 10, 30, 60, 100, 150, 200 and 300 at a final concentration of 1 μg plasmid DNA per well. Then, after 4 hours incubation at 37 °C in a humidified atmosphere, serum was added in the medium, and the cells were further incubated for 48 hours, in the same conditions. The expression of EYFP was followed by both fluorescence microscopy and flow cytometry. As controls, cells incubated in the normal culture medium (negative control), and cells transfected with pEYFP using branched 25 kDa PEI and a commercially available transfection reagent (SuperFect®, from Qiagen) following the producer's instructions (positive control), were used.

The fluorescence imaging technique has been used to give evidence of the success of the transfection induced by PEI/pEYFP and cD_4^H–AGE–PEI/pEYFP polyplexes. The expression of reporter fluorescent protein in HEK 293T cells was visualized 48 hours after transfection, using an Olympus IX81 inverted microscope equipped with filter sets specific for detection of FITC/GFP fluorescence (excitation/bandwidth: 480 nm/20 nm; emission/bandwidth: 510 nm/20 nm). The images were captured with a CCD camera, using CellSense Dimensions software application.

Flow cytometry analyses were performed using a Gallios, Becton Dickinson flow cytometer. Forty eight hours post-transfection, HEK 293T cells were harvested by trypsinization and analyzed to determine the percentage of transfected (EYFP-positive) cells, and the mean fluorescence intensity (MFI) of the EYFP signal. The fluorescence of the transfected cells was detected in the FL1 channel (530 nm), after excitation with the blue laser (488 nm). The transfection efficiency was calculated as the percentage of cells that express the EYFP, relative to the total number of cells investigated by flow cytometry, after counting 10 000 events for each transfected sample. At least three independent experiments were performed in triplicate for each experiment.

Molecular modeling was performed by molecular orbital calculations at the level of PM3 theory, using the MOPAC software application,[61,62] in order to optimize the geometry of the cD_4^H–AGE–PEI conjugate. The interaction between the conjugate and the DNA helix was studied by molecular dynamics simulation, in an explicit solvent environment (water), using the YASARA-Structure software package, version 14.12.2,[45,46,63] which employs an automatic parameterization procedure (termed ''AutoSMILES'') for the unknown structures. The simulated DNA was a Drew–Dickerson dodecamer $d(CGCGAATTCGCG)_2$ containing 24 nucleotides, with a total charge of −26 (fully deprotonated) in aqueous solution at a pH of 7.4. In the case of the cD_4^H–AGE–PEI conjugate, amine groups of PEI were considered to have a protonation ratio of 50%, at the physiological pH. In these conditions, the conjugate represents a polycation, which carries a total charge of +26 in aqueous solution, at pH 7.4.

Conclusion

The present work describes the design principles, the synthesis, the physical–chemical characterization, and the transfection efficacy evaluation, of a small volume carrier molecule able to collectively build cargocomplexes with DNA. Particularly, the carrier is a conjugate between a cyclic siloxane molecule and, on average, 3.76 molecules of 2 kDa branched polyethyleneimine, connected together by a short spacer. As a macromolecule, the conjugate is a flexible amphipathic structure, consisting of a hydrophobic core and polycationic branches. It has the propensity to adopt an asymmetric spatial conformation, favorable both to the electrostatic interaction with DNA, and to expose the hydrophobic moiety, which becomes a compatibilizing interface against lipidic barriers.

The transfection ability of the synthesized conjugate was tested by collective complexation with the pEYFP plasmid, which comprises a reporter gene that, if successfully transfected into viable cells, induces the expression of a fluorescent protein, thus permitting the objective quantification of the transfection efficacy. *Per se*, the carrier molecule proved to be non-cytotoxic, blood compatible, and able to fully associate with the plasmid at N/P ratios of 15 and larger. Transfection yields better than 30% could be obtained starting from N/P ratios of 60. The parallel performed tests showed that the developed carrier (cD_4^H–AGE–PEI conjugate) is more effective in inducing transfection when compared to the commercial SuperFect® reagent.

Based on the proven performances of the cD_4^H–AGE–PEI conjugate, we consider that it represents a valuable non-viral gene vector, able to collectively collaborate, on the molecular level, to transfect large nucleic acid molecules, of biological significance in controlling genetic information storage and expression.

Acknowledgements

This work was supported by a grant of the Romanian National Authority for Scientific Research, CNCS – UEFISCDI, project number PN-II-ID-PCCE-2011-2-0028. The authors are also grateful to Dr Cristian Varganici for thermal analysis, Dr Laura Ursu for providing high quality AFM images and Adina Coroaba, PhD student, for performing XPS analysis.

Notes and references

1 S. P. Wong, O. Argyros and R. P. Harbottle, Non-Viral Vectors for Gene Therapy: Physical Methods and Medical Translation, in *Advances in Genetics Series*, ed. L. Huang, D. Liu and E. Wagner, Academic Press, London, 1st edn, 2015, ch. 5, vol. 89, pp. 113–152.

2 B. Alberts, A. Johnson, J. Lewis, D. Morgan, M. Raff, K. Roberts and P. Walter, in *Molecular Biology of the Cell*, ed. D. Schanck, A. Bochicchio, G. Lucas, S. Granum Lewis and E. Zayatz, Garland Science, New York, 6th edn, 2015, ch. 4, pp. 173–237.

3 I. Trapani, P. Colella, A. Sommella, C. Iodice, G. Cesi, S. de Simone, E. Marrocco, S. Rossi, M. Giunti, A. Palfi, G. J. Farrar, R. Polishchuk and A. Auricchio, *EMBO Mol. Med.*, 2014, **6**(2), 194–211.

4 F. Pampinella, M. Pozzobon, E. Zanetti, P. G. Gamba, I. McLachlan, M. Cantini and L. Vitiello, *Neurol. Sci.*, 2000, **21**, S967–S969.

5 G. Kaul and M. Amiji, in *Tissue Engineering and Novel Delivery Systems*, ed. M. J. Yaszemski, D. J. Trantolo, K. -U. Lewandrowski, V. Hasirci, D. E. Altobelli and D. L. Wise, Marcel Dekker Inc., New York, 2004, ch. 16, pp. 415–459.

6 R. I. Zhdanov, O. V. Podobed and V. V. Vlassov, *Bioelectrochemistry*, 2002, **58**, 53–64.

7 R. Goyal, S. K. Tripathi, S. Tyagi, R. K. Rama, K. M. Ansari, Y. Shukla, D. K. Chowdhuri, P. Kumar and K. C. Gupta, *Eur. J. Pharm. Biopharm.*, 2011, **79**, 3–14.

8 X. Zhang, Y. Duan, D. Wang and F. Bian, *Carbohydr. Polym.*, 2015, **122**, 53–59.

9 S. M. Farkhani, A. Valizadeh, H. Karami, S. Mohammadi, N. Sohrabi and F. Badrzadeh, *Peptides*, 2014, **57**, 78–94.

10 F. Wang, Y. Wang, X. Zhang, W. Zhang, S. Guo and F. Jin, *J. Controlled Release*, 2014, **174**, 126–136.

11 W. Qu, S.-Y. Qin, Y. Kuang, R.-X. Zhuoa and X.-Z. Zhang, *J. Mater. Chem. B*, 2013, **1**, 2147–2154; H. Parhiz, W. T. Shier and M. Ramezani, *Int. J. Pharm.*, 2013, **457**(1), 237–259.

12 C. Aranda, K. Urbiola, A. M. Ardoy, J. M. García Fernández and C. O. Mellet, *Eur. J. Pharm. Biopharm.*, 2013, **85**(3 Pt A), 390–397.

13 M. S. Shim and Y. J. Kwon, *Adv. Drug Delivery Rev.*, 2012, **64**, 1046–1059.

14 H. Chen, X. Liu, Y. Dou, B. He, L. Liu, Z. Wei, J. Li, C. Wang, C. Mao, J. Zhang and G. Wang, *Biomaterials*, 2013, **34**, 4159–4172.

15 S. Browne, G. Fontana, B. J. Rodriguez and A. Pandit, *Mol. Pharmaceutics*, 2012, **9**(11), 3099–3106.

16 B. Newland, T. C. Moloney, G. Fontana, S. Browne, M. T. Abu-Rub, E. Dowd and A. S. Pandit, *Biomaterials*, 2013, **34**, 2130–2141.

17 K. Qamhieh and A. A. Khaleel, *Colloids Surf., A*, 2014, **442**, 191–198.

18 F. Wang, Y. Wang, H. Wang, N. Shao, Y. Chen and Y. Cheng, *Biomaterials*, 2014, **35**, 9187–9198.

19 X. Du, B. Shi, Y. Tang, S. Dai and S. Z. Qiao, *Biomaterials*, 2014, **35**, 5580–5590.

20 A. Saraf, M. C. Hacker, B. Sitharaman, K. J. Grande-Allen, M. A. Barry and A. G. Mikos, *Biomacromolecules*, 2008, **9**, 818–827.

21 B. Sitharaman, T. Y. Zakharian, A. Saraf, P. Misra, J. Ashcroft, S. Pan, Q. P. Pham, A. G. Mikos, L. J. Wilson and D. A. Engler, *Mol. Pharmaceutics*, 2008, **5**(4), 567–578.

22 C. M. Uritu, C. D. Varganici, L. Ursu, A. Coroaba, A. Nicolescu, A. I. Dascalu, D. Peptanariu, D. Stan, C. A. Constantinescu, V. Simion, M. Calin, S. S. Maier, M. Pinteala and M. Barboiu, *J. Mater. Chem. B*, 2015, **3**, 2433–2446.

23 H. Huang, H. Yu, G. Tang, Q. Wang and J. Li, *Biomaterials*, 2010, **31**(7), 1830–1838.

24 H. Chen, X. Liu, Y. Dou, B. He, L. Liu, Z. Wei, J. Li, C. Wang, C. Mao, J. Zhang and G. Wang, *Biomaterials*, 2013, **34**(16), 4159–4172.

25 C. Bienvenu, Á. Martínez, J. L. Jiménez Blanco, C. Di Giorgio, P. Vierling, C. Ortiz Mellet, J. Defayec and J. M. García Fernández, *Org. Biomol. Chem.*, 2012, **10**(29), 5570–5581.

26 B. Mendrek, Ł. Sieroń, M. Libera, M. Smet, B. Trzebicka, A. L. Sieroń, A. Dworak and A. Kowalczuk, *Polymer*, 2014, **55**, 4551–4562.

27 T. Dudzina, N. von Goetz, C. Bogdal, J. W. H. Biesterbos and K. Hungerbühler, *Environ. Int.*, 2014, **62**, 86–94.

28 T. C. Kendrick, B. Parbhoo and J. W. White, in *The Chemistry of Organic Silicon Compounds*, ed. S. Patai and Z. Rappoport, John Wiley & Sons Ltd., New York, 1989, ch. 21, vol. 1, pp. 1289–1361.

29 Z. Wang, Y. Zhao, L. Ren, L. Jin, L. Sun, P. Yin, Y. Zhang and Q.-Q. Zhang, *Nanotechnology*, 2008, **19**(44), 445103.

30 X. Tian, F. Wei, T. Wang, D. Wang, J. Wang, X. Lin, P. Wang and L. Ren, *Mater. Lett.*, 2012, **68**, 94–96.

31 X.-H. Tian, Z.-G. Wang, H. Meng, Y.-H. Wang, W. Feng, F. Wei, Z.-C. Huang, X.-N. Lin and L. Ren, *Int. J. Nanomed.*, 2013, **8**, 865–876.

32 S. K. Tripathi, V. P. Singh, K. C. Gupta and P. Kumar, *J. Mater. Chem. B*, 2013, **1**, 2515–2524; J. C. Sunshine, M. I. Akanda, D. Li, K. L. Kozielski and J. J. Green, *Biomacromolecules*, 2011, **12**, 3592–3600.

33 T. V. Timofeeva, I. L. Dubchak, V. G. Dashevsky and Y. T. Struchkov, *Polyhedron*, 1984, **3**(9/10), 1109–1119.

34 G. Lin, H. Zhang and L. Huang, *Mol. Pharmaceutics*, 2015, **12**(2), 314–321.

35 E. W. Colvin, *Silicon Reagents in Organic Synthesis*, Academic Press, London, 1988.

36 D. Schinzer, in *Organic Synthesis Highlights II*, ed. H. Waldmann, Wiley-VCH Verlag GmbH & Co. KgaA, Weinheim, 1995, part I(C), pp. 123–128.

37 R. Tacke and U. Wannagat, in *Bioactive Organo-Silicon Compounds*, ed. M. J. S. Dewar, K. Hafner, E. Heilbronner, S. Ito, J. -M. Lehn, K. Niedenzu, C. W. Rees, K. Schäfer and G. Wittig, Topics in Current Chemistry, Springer-Verlag, Berlin, 1979, vol. 84, pp. 1–75.

38 V. Harabagiu, M. Pinteala, C. Cotzur, M. N. Holerca and M. Ropot, *J. Macromol. Sci., Part A: Pure Appl.Chem.*, 1995, **32**, 1641–1648.

39 D. R. Anderson, in *Analysis of Silicones*, ed. A. L. Smith, Wiley Interscience, New York, 1974, ch. 10, pp. 247–286.

40 G. Socrates, *Infrared and Raman Characteristic Group Frequencies: Tables and Charts*, John Wiley and Sons Ltd, Chichester, UK, 3rd edn, 2001.

41 V. V. Nedel'ko, B. L. Korsunskii, F. I. Dubovitskii and G. L. Gromova, *Polym. Sci. U.S.S.R.*, 1975, **17**(7), 1697–1703.

42 A. K. Varkouhi, M. Scholte, G. Storm and H. J. Haisma, *J. Controlled Release*, 2011, **151**, 220–228.

43 J.-L. Burgot, *Ionic Equilibria in Analytical Chemistry*, Springer Science + Business Media, LLC, New York, 2012.

44 T. Nogrady and D. F. Weaver, *Medicinal Chemistry. A Molecular and Biochemical Approach*, Oxford University Press, Oxford, UK, 3rd edn, 2005.

45 E. Krieger, G. Koraimann and G. Vriend, *Proteins*, 2002, **47**, 393–402.

46 E. Krieger, K. Joo, J. Lee, J. Lee, S. Raman, J. Thompson, M. Tyka, D. Baker and K. Karplus, *Proteins*, 2009, **77**(S9), 114–122.

47 O. M. Becker, in *Computational Biochemistry and Biophysics*, ed. O. M. Becker, A. D. MacKerell, B. Roux and

M. Watanabe, Marcel Dekker Inc., New York, 2001, ch. 4, pp. 69–90.
48 C. Stan Tsai, *An Introduction to Computational Biochemistry*, Wiley-Liss, New York, 2002.
49 D. A. Tomalia, J. B. Christensen and U. Boas, in *Dendrimers, Dendrons, and Dendritic Polymers: Discovery, Applications, and the Future*, Cambridge University Press, Cambridge, UK, 2012, ch. 5.3, pp. 203–214.
50 *US Pat.,* 7 192 744, 2007.
51 M. X. Tang, C. T. Redemann and F. C. Szoka Jr., *Bioconjugate Chem.*, 1996, **7**, 703–714.
52 H. Arima, in *Non-viral Gene Therapy: Gene Design and Delivery*, ed. K. Taira, K. Kataoka and T. Niidome, Springer-Verlag, Tokyo, 2005, ch. 1, pp. 75–86.
53 M. Ogris, in *Polymeric Gene Delivery. Principles and Applications*, ed. M. M. Amiji, CRC Press LLC, Boca Raton, FL, 2004, ch. 7, pp. 97–106.
54 O. Boussif, F. Lezoualc'h, M. A. Zanta, M. D. Mergny, D. Scherman, B. Demeneix and J.-P. Behr, *Proc. Natl. Acad. Sci. U. S. A.*, 1995, **92**, 7297–7301.
55 B. A. Demeneix, M. Ghorbel and D. Goula, in *Gene Targeting Protocols*, ed. E. B. Kmiec, Methods in Molecular Biology, Humana Press Inc., Totowa, NJ, 2000, ch. 2, vol. 133, pp. 21–35.
56 OECD 1995, Test No. 107, *OECD Guidelines for the Testing of Chemicals*, *Section 1*, OECD Publishing, Paris, 1995, DOI: 10.1787/9789264069626-en.
57 A. Leo, C. Hansch and D. Elkins, *Chem. Rev.*, 1971, **71**(6), 525–616.
58 F. Ungaro, G. De Rosa, A. Miro and F. Quaglia, *J. Pharm. Biomed. Anal.*, 2003, **31**, 143–149.
59 L. Kupcsik, in *Mammalian Cell Viability: Methods and Protocols*, ed. M. J. Stoddart, Methods in Molecular Biology, Humana Press, Springer Science + Business Media, New York, 2011, ch. 3, vol. 740, pp. 13–19.
60 G. Creusat, A.-S. Rinaldi, E. Weiss, R. Elbaghdadi, J.-S. Remy, R. Mulherkar and G. Zuber, *Bioconjugate Chem.*, 2010, **21**(5), 994–1002.
61 J. J. P. Stewart, *MOPAC2012, Version 14.139W*, Stewart Computational Chemistry, Colorado Springs, CO, 2012, available from URL: http://openmopac.net.
62 J. D. C. Maia, G. A. U. Carvalho, C. P. Mangueira, S. R. Santana, L. A. F. Cabral and G. B. Rocha, *J. Chem. Theory Comput.*, 2012, **8**(9), 3072–3081.
63 YASARA, http://www.yasara.org/, accessed January 2014.